Late Cretaceous Channel Flow In Western Arizona: Implications For The Ancestral Evolution of Metamorphic Core Complexes

Thomas N Lamont[1*], Shane Scoggin[2], Johannes Haemmerli[2], Gabe Epstein[3], Alex Scandore[1], Meaghan Boyle[1], Michael Wells[1]

[1*]Department of Geoscience, University of Nevada Las Vegas, 4505 S. Maryland Parkway, Las Vegas, 89154, NV, USA.
[2]Department of Geology, Washington State University, Pullman, 99163, WA, USA.
[3]School of Earth and Sustainability, Northern Arizona University, Flagstaff, 86001, AZ, USA.

*Corresponding author(s). E-mail(s): thomas.lamont@unlv.edu;

Abstract

The origin of ancestral 'extensional' shear fabrics in metamorphic core complexes (MCCs) in the Colorado River Extensional Corridor remains a tectonic mystery. Here we show that Late-Cretaceous metamorphic rocks and migmatites in the Harcuvar-Harquahala and Granite Wash Mountains MCCs reached peak metamorphic conditions of ca. 0.75 GPa and 780°C and were extruded towards the SW onto lower grade metamorphic rocks via 'channel flow' between ca. 76–70 Ma, ∼40 Myrs before regional extension. The channel is bounded by a top-NE 'extensional' roof shear zone and a top-SW thrust-sense base, associated with an inverted metamorphic gradient. U-(Th)-Pb and Rb-Sr geochronology confirms that shearing at the roof and base occurred concurrently. To explain these features, we propose that low-angle subduction of the Farallon plate released volatiles directly into the base of the North American crust, which induced water-fluxed crustal melting and rheological weakening, facilitating flow of deep crustal rock to shallower depths. Consequently, ancestral 'extensional' fabrics in MCCs may represent the roof of an extruding channel formed in an overall contractional setting.

Keywords: Metamorphic Core Complex, Channel Flow, Low-Angle Subduction, Water-Fluxed Crustal Melting, Laramide Orogeny

INTRODUCTION

Metamorphic core complexes (MCCs) are characteristic features of extensional continental tectonics and are defined as having a high-grade metamorphic footwall that is separated from an unmetamorphosed hanging wall by a low angle normal fault or ductile shear zone (Figure 1; Teyssier and Whitney, 2002; Whitney et al. 2013; Platt et al. 2014). However, within the footwall of many MCCs across the North American Cordillera and Alpine-Himalayan belt, the timing of peak metamorphism and ductile shearing significantly pre-dates the onset of regional crustal extension and sedimentary basin formation in the hanging wall of the detachment (Figure 2). Kyanite and sillimanite grade gneisses, migmatites and sometimes granulite facies rocks exposed at the deepest structural levels of many MCC footwalls often demonstrate clockwise pressure temperature time (P-T-t) paths associated with burial and heating of rock in contractional settings, which is followed by periods of decompression and exhumation, prior to regional extension (Searle and Lamont, 2019; Lamont et al. 2020; Hallet and Spear, 2014; Wells et al., 2020). Shear fabrics associated with this ancestral phase of exhumation are preserved within many MCCs, and are cut or captured by a younger normal fault responsible for final MCC exhumation to the Earth's surface (Hodges and Walker, 1992; Wells and Hoisch, 2008; Searle and Lamont, 2019; Lamont et al. 2020a; Zuza et al. 2022). This capture of older, higher temperature fabrics is especially prevalent in the MCCs of the Colorado River Extensional Corridor (CREC; Davis and Lister, 1988; Spencer and Reynolds, 1990; Singleton and Mosher, 2012). This ancestral phase of exhumation requires advection of deep crustal material before the main phase of extension. However, the origin of ancestral shear fabrics preserved within the footwalls of many MCCs remains poorly understood. Because these fabrics predate strain indicators associated with final exhumation, they may provide important insights into the dynamic strain and stress regimes that operated within the continental lithosphere during orogenesis.

One possibility is that the ancestral shear fabrics represent normal faulting and crustal extension either during orogenic collapse (Dewey, 1988) or in a locally extensional setting within a zone of overall convergence (Dalmayrac and Molnar, 1981; Figure 3A). Evidence in support of these extensional hypotheses would be preservation of only normal-sense shear indicators coeval with decompression. In other words, as the rocks moved upward towards the earth's surface from higher pressure to lower pressure, their older high-pressure minerals should have been overprinted or replaced by lower-pressure mineral assemblages that are associated with only normal sense shear indicators. Pure shear, uniform (with depth) lithospheric extension increases the crustal geotherm at a rate proportional to conductive heat-loss due to exhumation of rock at all crustal levels (e.g., Ruppel et al., 1988). This does not cause any net-heating of rock, but rather cooling of rock or delayed cooling during exhumation, depending on the magnitudes and rates of extension. Depth dependent extension, with smaller magnitudes of extension in the crust (β) and larger magnitudes of extension in the mantle (γ), results in deep crustal heating (e.g, Royden and Keen, 1980; Royden, 1996; Lamont et al. 2023). Compared to uniform extension, increasing magnitudes of extension with depth would produce: A) a higher metamorphic field gradient increasing with structural depth beneath the detachment, and B) alkalic volcanism due to

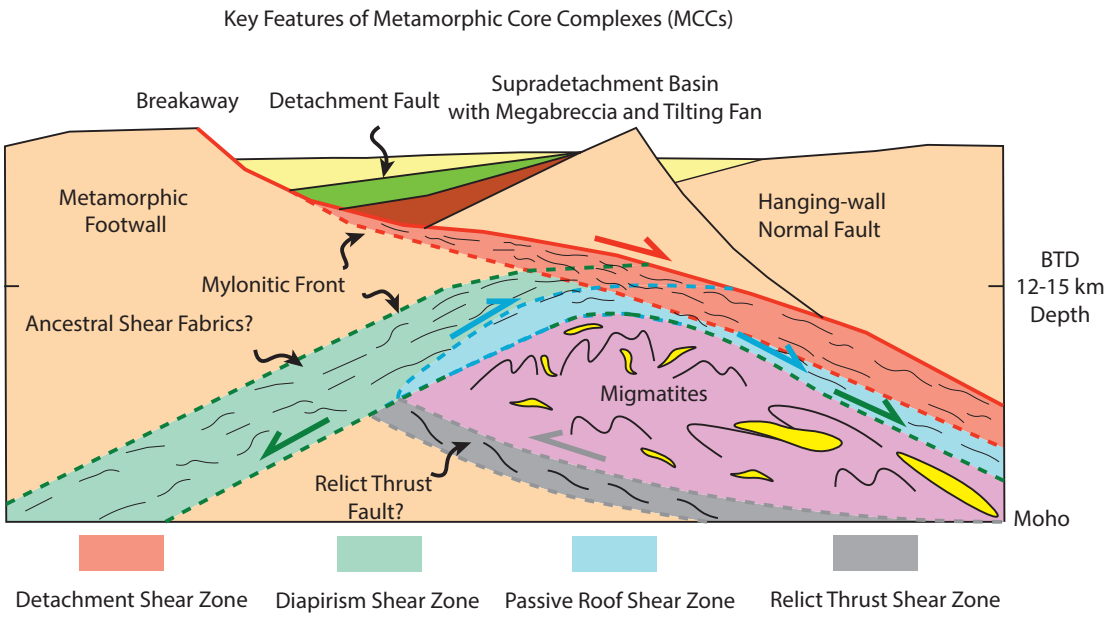

Fig. 1: Cartoon sketch showing the key features of metamorphic core complexes (MCCs) after Zuza et al. (2022). Note the ancestral shear fabrics and shear zones within the metamorphic footwall which are discordant to the detachment fault.

melting the lithospheric mantle from increased asthenospheric heat flow. Both extensional cases would also lead to development of a sedimentary basin in the the hanging wall of the detachment fault. Perplexingly, in most MCCs, such upper crustal extensional features and volcanism are not preserved at the time of peak metamorphism and ductile shearing (Hodges and Walker, 1992). A possible explanation is a blind extensional allochthon model, whereby the mid-crust flows laterally bound by shear zones with opposing shear senses, leaving thinner-crust in its wake (Hodges and Walker, 1992). However, the absence of these features and structural relationships cast doubt on an overall extensional origin for the ancestral shear fabrics and may challenge the interpretation that they formed in an overall extensional tectonic setting.

Another possibility is that these shear fabrics result from diapirism (Zuza and Cao, 2022; Figure 3B). In this model, vertical flow of low viscosity and lower density partially molten lower crust occurs due to the development of a Rayleigh-Taylor instability. According to this model, one would expect to see chaotically deformed rocks within a gneiss or migmatite dome that is bound by radially divergent shear senses and lineations and steep fabrics along its margins due to upward flow of deep crustal material towards the Earth's surface. Diapirism could also occur in a tectonically quiescent setting after crustal thickening and before regional extension, as deformation is driven

by buoyancy contrasts likely due to partial melting of the mid to lower crust. However, many MCCs show uni-directional shear indicators and shallow-sub horizontal plunging lineations (Lamont et al. 2020a), inconsistent with this model.

Alternatively, ductile extrusion of high-grade metamorphic rocks or 'channel flow' can explain the exhumation of rocks and the development of 'extensional' shear fabrics in a wholly contractional setting (Burchfield and Royden, 1985; Beaumont et al. 2001; Searle et al. 2004; Godin et al. 2006; Searle and Lamont, 2019; Figure 3C). This model is defined as flow of a weak, ductile layer between relatively rigid, yet deformable, material above and below. The channel's lower boundary is defined by a thrust fault or ductile shear zone, while its upper boundary consists of a normal fault or extensional shear zone with a fixed hanging wall (Means, 1989), that operated simultaneously. Because weak ductile material flows between relatively fixed lithologies above and below, the upper and lower channel boundaries develop opposite shear senses that operated simultaneously. This flow also moves hot, deep crustal rocks relative to cooler rocks, which results in an inverted metamorphic gradient near the base of the channel and a right-way up metamorphic gradient in the upper part of the channel. Two end-member models can describe the relative motion of ductile rocks within the channel. The Poiseuille flow (pipe flow) model, suggests the highest flow velocities occur in the middle of the channel, while the Couette flow model suggests the highest velocities occur either along the top or the base of the channel (Law et al. 2004, 2011; Grujic et al. 1996, Klemperer 2006).

Channel flow or ductile extrusion has been well documented in subduction complexes that expose high-pressure metamorphic rocks juxtaposed against rocks that obtained much lower metamorphic grades as thrust bound nappes or blocks within a mélange (England and Holland, 1979; Geyra et al. 2002; Agard et al. 2009; Searle and Lamont, 2019; Lamont et al. 2020b). In these settings, return flow is driven by the positive buoyancy contrast between subducted crustal material that is detached from the down-going plate and the surrounding mantle (e.g., England and Holland, 1979). However, our understanding of how such a mechanism operates in continental crustal settings associated with regional metamorphism remains limited, particularly where buoyancy contrasts are less pronounced (e.g., Grujic et al. 1996; Beaumont et al. 2001; Searle et al. 2003; Law et al. 2004, 2011; Godin et al. 2006).

The Greater Himalayan Series (GHS) in the high Himalaya is the best representation of where the channel flow model may account for the opposite shear senses and metamorphic field gradients of once mid crustal metamorphic rocks. The GHS is bounded along the base by the Main Central Thrust (MCT) ductile shear zone, a south-verging thrust that was concomitant with an inverted metamorphic field gradient (Hubbard 1989; Searle et al. 2006, 2018; Jessup et al. 2008a, b). In contrast, the north-dipping South Tibetan Detachment (STD) low-angle normal faults were concomitant with right-way up metamorphic isograds along the top (Caby, 1983; Burchfiel et al. 1992; Searle et al. 2003; Law et al. 2004, 2011; Cottle et al. 2007, 2015; Searle 2010; Waters et al. 2019). Both the MCT and STD ductile shear zones were active simultaneously (Godin et al. 2006) as supported by high-temperature ductile fabrics and ages of metamorphism throughout the GHS above the MCT zone and beneath the STD zone. The migmatite–leucogranite zone along the upper part of the GHS

records melting and deformation associated with southward-verging transport (Cottle et al. 2009; Searle et al. 2010). It is proposed that southward directed flow was driven by horizontal pressure gradients from gravitational potential energy gradients, as well as a denudation front (Beaumont et al. 2001) due to rheological weakening associated with in-situ crustal melting as documented by GHS migmatites and leucogranites (Yang et al. 2019).

The retro-wedge within the East Greenland Caledonides is another, albeit lesser studied, example of channel flow or ductile extrusion (e.g. Hodges, 2016). Here, mid-crustal upper amphibolite facies metamorphic rocks and migmatites (Gilotti et al. 2008; Johnston & Kylander-Clark, 2013) (referred to as the 'infrastructure') is separated from low-grade metamorphic rocks in the foreland by westward verging thrust faults (Leslie and Higins, 2008), which in some places have been reactivated as extensional detachments (e.g., Andresen et al. 2007, White & Hodges 2002). In contrast, the roof shear zone, that separates the upper amphibolite facies 'infrastructure' in the footwall from low grade metamorphic and sedimentary rocks (referred to as the 'suprastructure') in the hanging wall is an eastward dipping shallowly dipping normal fault - The Fjord Region Detachment (FRD) (Andresen et al. 1998; Hartz & Andresen 1995; Hartz et al. 2000, 2001; Strachan 1994; Strachan & Martin 2001; Hodges et al. 2016).

Here, we synthesize the field relationships and present new structural interpretation and geochronology data to better understand the geodynamic processes that operated within the metamorphic footwall of Harcuvar-Harquahala-Granite Wash Mountains MCCs within the North American Cordillera at a latitude near ∼34 °N. We propose that the Hercules, Centenial and Harquahala Thrusts in the Harcuvar, Harquahala, and Granite Wash Mountains of western Arizona represent the lower boundary of a ductile channel. High-grade metamorphic rocks, migmatites, and leucogranites structurally above these faults were transported southwestward by Late Cretaceous channel flow during the onset of low-angle subduction of the Farallon Plate. These new data challenge existing interpretations and provide critical new constraints on the origin of ancestral subhorizontal 'extensional' shear fabrics preserved in metamorphic core complexes globally.

Geology of the Harcuvar Harquahala and Granite Wash Mountains

The Harcuvar, Harquahala and Granite Wash Mountains are a series of MCCs located within the Colorado River extensional corridor of western Arizona in the hinterland of the Sevier-Laramide Orogen. These ranges are elongate domes with NE-SW trending long axes and are bound by NE plunging Miocene extensional detachment faults including the Bullard and Eagle Eye Detachment faults (Reynolds and Spencer, 1989; Reynolds et al. 1993). The Bullard and Eagle Eye detachment faults separate the unmetamorphosed Miocene volcanic rocks in the hanging walls from their metamorphic footwalls. (U-Th)/He zircon, Ar-Ar and Rb-Sr thermochronology has shown the extensional detachment faults were active from ca. 22 Ma to ca. 16 Ma (Richard et al., 1990; Singleton et al. 2014; Wong et al. 2023) and were responsible for the final exhumation of the MCCs to the Earth's surface. However, beneath the extensional

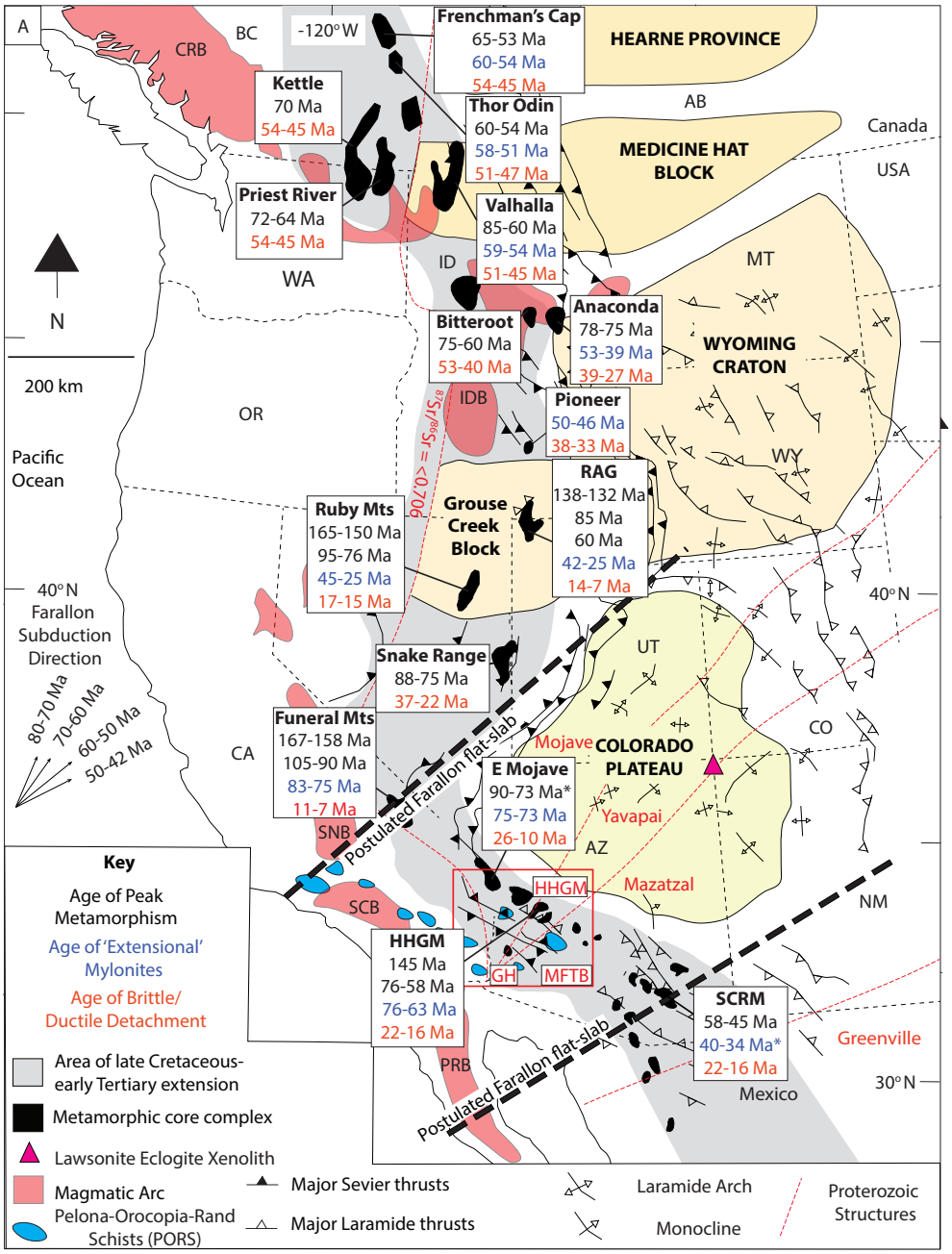

Fig. 2: Summary map of the SW USA showing ages of peak metamorphism and timing of ductile extensional shear fabrics and low temperature thermochronology related to timing of brittle extension. Location of Maria Fold Thrust Belt (MFTB), Harquahala-Harcuvar-Granite Wash Mountains (HHGM), Gavilan Hills (GH), Raft-River Albion, Grouse Creeke Mountains (RAG), SCRM (Santa Catalina-Rincon Mountains). See supplementary material for a complete compilation and list of references.

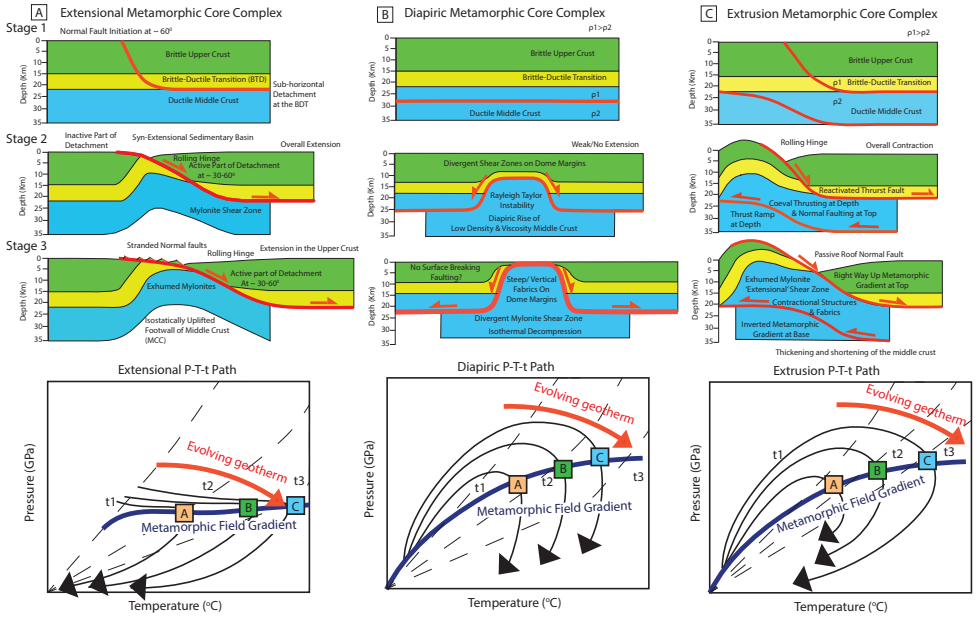

Fig. 3: Models for ancestral shear fabrics within the footwall of MCCs. A) Ductile shearing associated with a crustal scale detachment fault during regional extension, expected P-T path involving isobaric heating followed by exhumation or delayed cooling during exhumation. B) Ductile shearing on margins of a crustal scale diapir, that formed as a result of a Rayleigh Taylor instability, and expected P-T path involving isothermal decompression, C) Ductile shearing associated with a syn-convergent extrusion with a thrust fault at the base and an extensional detachment at the top of the extruding channel or wedge, and expected P-T-t path involving burial and heating from contraction followed by decompression and cooling due to extrusion related exhumation placing deeper and hotter rocks to top of shallower cooler rocks.

detachments, within the metamorphic footwall, a section of mid to lower crust of ∼60 km structural thickness is exposed.

This crustal section comprises high-grade metamorphic rocks including kyanite and sillimanite bearing migmatites, Proterozoic gneisses and Late Cretaceous-Paleocene peraluminous and metaluminous granites. These high grade metamorphic and Proterozoic basement rocks belong to the overthrusted crystalline southwest verging thrust sheets that define the Maria Fold-Thrust Belt (MFTB), a characteristic Laramide contractional feature in western Arizona and south east California (Reynolds et al. 1987; Spencer & Reynolds, 1990; Richard et al. 1994). The MFTB is an east-west trending belt of greenschist-amphibolite facies metamorphic rocks characterized by largely south-vergent folds and ductile shear zones that place Jurassic and Proterozoic crystalline rocks over Paleozoic and Mesozoic sedimentary and volcanic rocks correlative to strata observed on the Colorado Plateau and in southeastern Arizona (Spencer and Reynolds, 1990). $^{40}Ar/^{39}Ar$ step-heating analyses show the MFTB underwent regional metamorphism between ca. 90-80 Ma, likely due to overthrusting of basement

nappes (Knapp & Heizler, 1987). A deformed diorite, dated at ca. 86 Ma by U-Pb zircon geochronology (Saleem, 2009) and a granodiorite in the Coxcomb Mountains that cuts the McCoy Mountains Formation at ca. 73.5 Ma (Barth et al. 2004), indicate that thrusting occurred during the Late Cretaceous. Despite these dates, many questions remain, such as the precise timing and style of deformation and metamorphism within the MFTB and whether this influenced subsequent MCC development. Below we summarize the key geological features along a SW-NE transect through the Granite Wash, Harquahala and Harcuvar Mountains and integrate new thermobarometry and geochronology of deformation and metamorphism with previous literature data to provide new insights into the MFTB and the formation of these MCCs.

RESULTS

Field Relationships, Thermobarometry and Geochronology

In the Granite Wash Mountains to the far SW of the study area, the McCoy Mountains Formation was deposited between ca. 129 Ma and ca. 73 Ma (Caylor et al. 2024) and overlies Jurassic volcanics and Mesozoic sediments. These rocks only show low grade metamorphic assemblages (muscovite-chlorite; Fig. 5J,K) and are folded into a SW verging syncline, suggesting a phase of Late Cretaceous contraction shortly after final sediment deposition. These rocks are overlain by a major SW verging thrust fault – The Hercules Thrust – that places Proterozoic basement granites, gneisses and migmatites on top of the lower grade Mesozoic greenschist facies rocks.

A sample of a McCoy Mountains metasediment in the immediate footwall of the Hercules Thrust is characterized by the greenschist facies assemblage comprising muscovite-chlorite-epidote-titanite-albite-quartz (Fig. 6G), which equilibrated at 0.36 ± 0.13 GPa and 503 ± 36 °C (Lamont et al. 2024; Fig. 8). In-situ Rb-Sr geochronology on syn-kinematic white mica from the same sample yielded a date of 71.7 ± 12.9 Ma (Lamont et al. 2024), suggesting upper greenschist facies metamorphic conditions occurred during SW directed thrusting.

In the immediate hanging wall of the Hercules Thrust, leucosomes (former melt) occur within the Proterozoic basement and show top-SW asymmetry (Fig. 5H). However, the Granite Wash Granodiorite (ca. 72.7 Ma; U-Pb zircon age; Chapman et al. 2018) and the Tank Pass Ms+Grt+Bt granite (ca. 74-64 Ma; U-Pb zircon; Bryant & Wooden, 2008; Wong et al. 2023) cross cut the Hercules Thrust zone, suggesting that SW directed movement on the Hercules Thrust ceased by ca. 72-70 Ma.

Along strike to the south in the Little Harquahala Mountains, a complete section of the Hercules Thrust zone is exposed. Here, the Hercules Thrust also places mylonitized Proterozoic Basement gneisses on top of Jurassic volcanics and McCoy metasediments (Spencer et al. 2024). Structurally above the Hercules Thrust sheet, the Centenial Thrust places a sheet of Proterozoic basement and Paleozoic and Mesozoic metasediments over Proterozoic basement. The local presence of garnet in some metasediments, suggests an increase in metamorphic grade up structural section. Continuing up section in the Harquahala Mountains, the Harquahala Thrust, places an additional thrust sheet of crystalline basement on top of Mesozoic metasediments and Proterozoic Harquahala Granite. Along the Harquahala Thrust, the Proterozoic basement assemblages

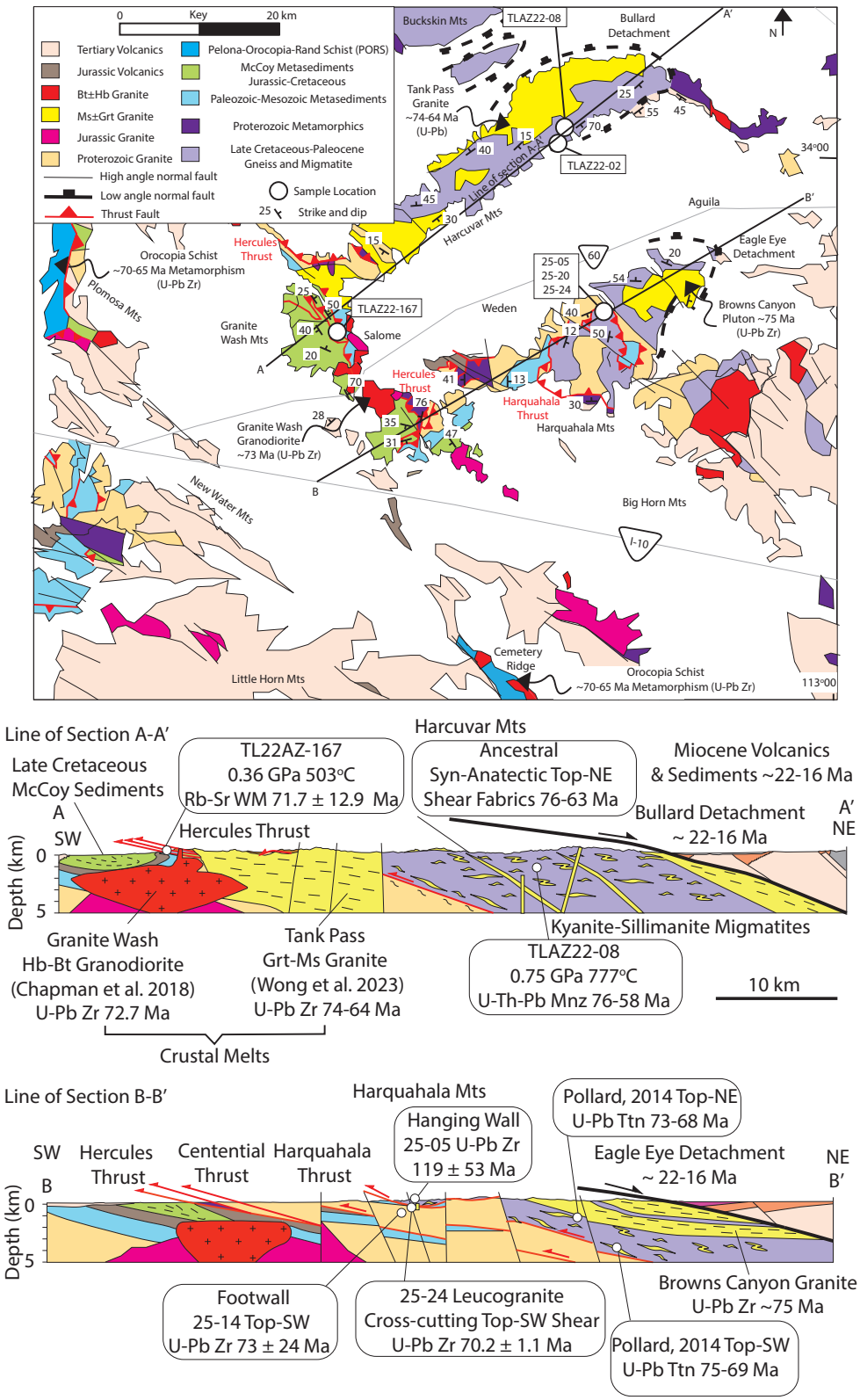

Fig. 4: Map and cross section of the Granite Wash, Harcuvar and Harquahala Mts showing sample locations, and the overall structure with inverted metamorphic field gradient at the base and top-SW shear fabrics and right-way up metamorphic field gradient and opposite top-NE shear fabrics at the top.

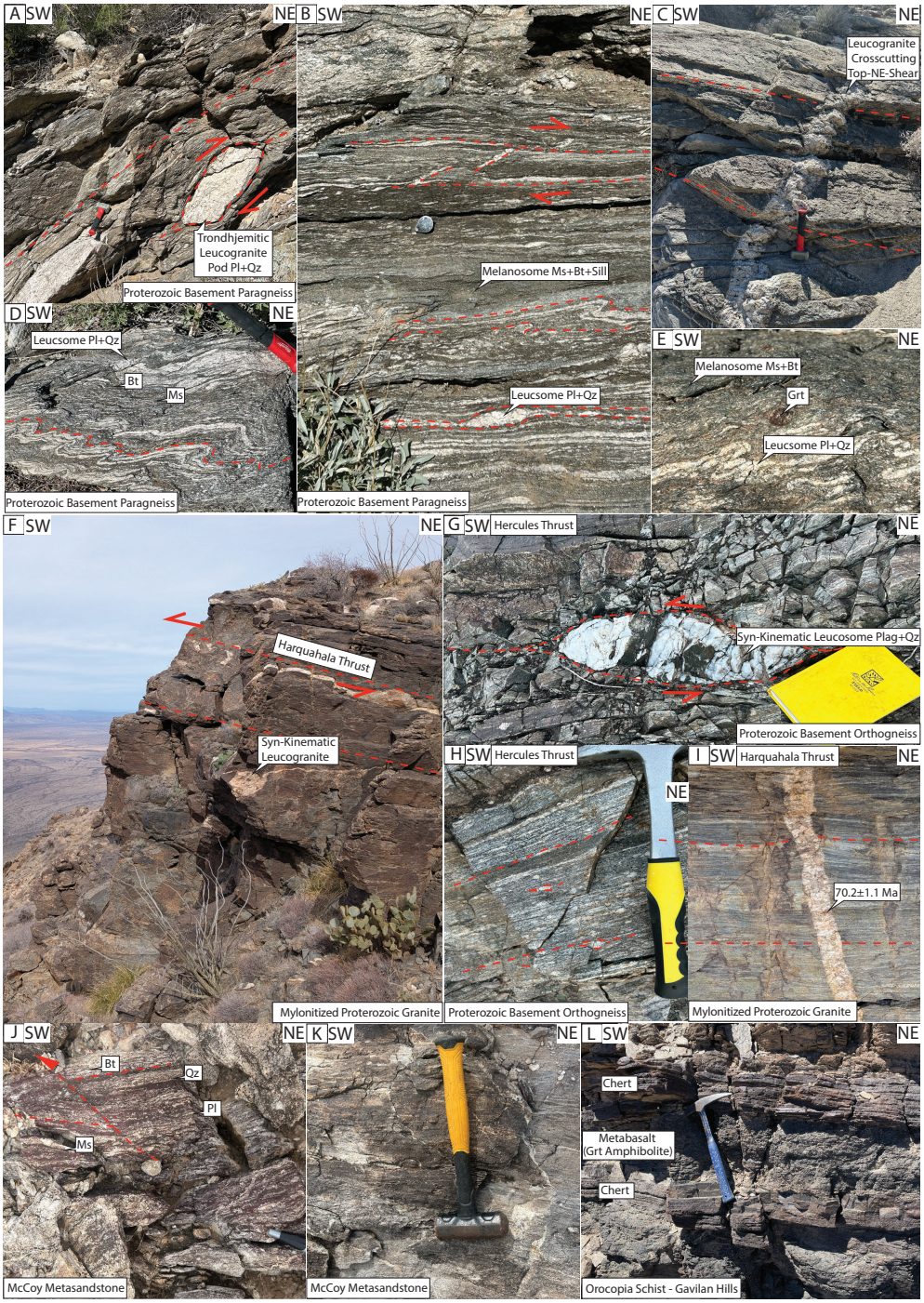

Fig. 5: Field photographs showing the main cross-cutting relationships of the Harcuvar, Harquahala and Granite Wash Mts. In particular top-NE shear occurred in the presence of partial melt at high structural levels, whereas top-SW shearing occurred at deeper structural levels, note the decreasing metamorphic grade with increasing structural depth. A-B) Top-NE shearing affecting anatectic features including leucosomes and leucogranite pods in the Harcuvar Mts. C) NNE-SSW trending steeply dipping leucogranite pegmatite dyke cross-cutting the top-NE shear fabrics. D-F) Leucosomes folded with a NE-trending vergence and shallow plunging NE-trending hinge lines. F) Syn-kinematic leucosomes and leucogranites aligned along the Harquahala Thrust. G) Asymmetric leucosome porphyroclast with top-SW shear sense, H) Mylonitized Proterozoic orthogneiss from the Hercules Thrust. I) Sample 25-24 leucogranite vein, cross-cutting the top-SW mylonite fabric on the Harquahala Thrust, J-K) Deformed greenschist facies Late Cretaceous McCoy metasediments in the footwall of the Hercules Thrust. L) Garnet Amphibolite mafic schist intercalated with metachert representing Farallon Plate ocean plate stratigraphy, from the Orocopia Schist in the Gavilan Hills.

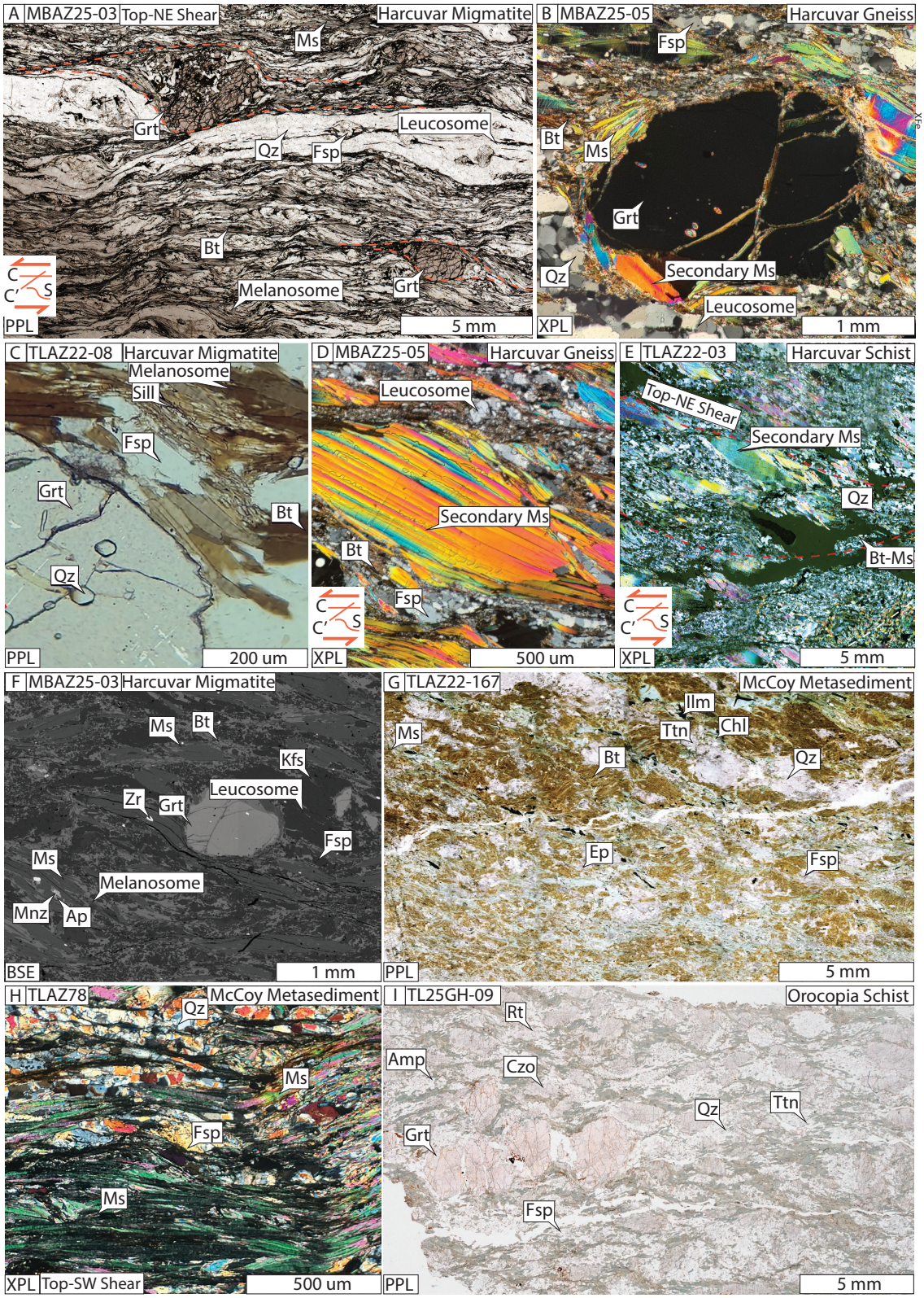

Fig. 6: Photomicrographs documenting petrography of A-E) Sillimanite migmatite in hanging wall of the Hercules Thrust, G-H) Greenschist facies McCoy metasediment in the footwall of the Hercules Thrust and I) Sample TL25GH-09, a garnet amphibolite from the Orocopia Schist at the Gavilan Hills.

are affected by intense mylonitization and locally partial melting. Shear sense indicators including sigma porphyroclasts and deformed leucosomes also show top-SW asymmetry, whereas some leucocratic veins and dykes cross-cut the foliation, clearly indicating that thrusting was coeval with anatectic conditions. Leucogranitic dike sample 25-24 which cross-cuts the mylonitic foliation in the footwall (Fig. 5I) yielded a zircon $^{238}U/^{206}Pb$ weighted mean age of 70.2 ± 1.1 Ma, suggesting top-SW thrusting ended by this time. Two additional samples, from the hanging wall (sample 25-05) and footwall (sample 25-14) of the Harquahala Thrust yield zircon U-Pb discordia lower intercept ages of 119 ± 53 Ma, and 73 ± 24 Ma respectively, which overlap with the weighted mean age of the cross-cutting dike. These ages also overlap with unpublished U-Pb titanite geochronology from shear zones with top-SW kinematics in the hanging wall between ca. 76-69 Ma (Pollard, 2014). Together, these data suggest that upper amphibolite facies metamorphism and movement along the Harquahala Thrust occurred at ca. 70 Ma.

Moving up structural section, in the hanging wall of the Harquahala Thrust near Brown's Canyon in the northeastern Harquahala Mountains, the abundance of leucosomes increases and some rocks show garnet and kyanite or sillimanite bearing mineral assemblages, that are pre-syn tectonic with respect to the foliation, indicating an inverted metamorphic field gradient. Along this section, the kinematic indicators also reverse to top-NE directed shear. Top-NE shearing also affects the peraluminous Brown Canyon granite dated at ca. 75 Ma (Pollard et al., 2014; Isachsen et al. 1999). Similar field relationships also occur in the Harcuvar Mountains, as migmatites and leucogranites crop out within Proterozoic basement protoliths to the NE of the ca. 74-64 Ma Tank Pass Granite (Wong et al. 2023).

Approximately 8 km above the Hercules Thrust in the Harcuvar Mountains, volumetrically abundant (locally >35% rock volume) leucosomes occur within paragneiss and amphibolite. The leucosomes have trondhjemitic (plagioclase-quartz) compositions and show diffuse boundaries (Figs. 5A-E and 6A). There is also minor (<1%) kyanite or sillimanite (Fig. 6C), and negligible peritectic k-feldspar (Fig. 6F) yet abundant secondary muscovite and biotite that occurs as mm-cm sized flakes (Fig. 6D-E). These observations are inconsistent with the migmatite petrogenesis being a product of muscovite dehydration melting above the solidus. This is because, during muscovite dehydration melting, k-feldspar, sillimanite and melt should have a stoichiometric ratio of 8/5/10 (Dyck et al. 2020). Furthermore, the trondhjemitic leucosome compositions and secondary muscovite implies that anatexis occurred by the addition of water, and resulted in the breakdown of plagioclase and k-feldspar (reaction 1 for a felsic protolith and reaction 2 for a mafic protolith).

$$(Felsic\ Protolith)\ Muscovite + Plagioclase + Quartz + H_2O -> Melt \quad (1)$$

$$(Mafic\ Protolith)\ Amphibole + Plagioclase + Quartz + H_2O -> Melt \quad (2)$$

Many of the leucosomes are ptygmatically folded with a NE-directed vergence, have sub-horizontal NE-trending hinge lines, and are sheared with top-NE/ENE kinematic indicators. Millimetric to centimetric sized flakes of secondary muscovite, that likely grew during melt crystallization, also show top-NE asymmetries, suggesting ductile shearing continued during cooling through the water-saturated solidus. All these features are consistent with partial melting occurring by the addition of water (Weinberg & Hasalova, 2015) during exhumation within a NE-dipping 'extensional' shear zone.

A sillimanite bearing migmatite (sample TLAZ22-08) and schist (TLAZ22-02) from the Central Harcuvar Mountains yielded U-(Th)-Pb monazite dates of ca. 76-58 Ma with elevated Gd/Yb ratios between ca. 73-60 Ma (Fig. 7), likely recording monazite growth in the presence of garnet (Spear & Pyle, 2002, 2010). Sample TLAZ22-08 records peak metamorphic conditions of 0.75 ± 0.08 GPa and 777 ± 36°C, which were calculated from garnet core compositions in equilibrium with biotite-sillimanite-plagioclase-quartz and minimal k-feldspar, whereas the garnet outer rim records 0.59 ± 0.08 GPa and 754 ± 24°C implying decompression above the solidus (Lamont et al. 2024; Fig. 8). Walsh et al. (2016) also reported U-(Th)-Pb monazite dates from the Harcuvar mountains between ca. 76-70 Ma and argue for a decompression P-T path from ca. 1.0-0.6 GPa, related to retrograde staurolite growth. U-Pb geochronology of syn-tectonic titanite within top-NE shear zones in the Harquahala Mountains gave dates between ca. 72-68 Ma (Pollard et al. 2014).

However, the top-NE shear fabrics and migmatite features are cross-cut by NNE-SSW and NNW-SSE trending Ms+Grt±Bt leucogranite and pegmatite dykes that have been dated between ca. 70-55 Ma (Isachsen et al. 1999; Wong et al. 2023; Fig. 5C). Integrating these data implies that high temperature top-NE shearing occurred before Miocene extension and in the presence of partial melt and during the decompression of rock between ca. 76-63 Ma.

During this same time interval, the Pelona-Orocopia-Rand Schists (PORS), exposed in the nearby Plomosa mountains, Cemetery Ridge and the Gavilan Hills in SE California (Figs. 2 and 4) were underplated directly beneath the base of the North American crust as a result of low angle subduction of the Farallon Plate between ca. 70-65 Ma (e.g. Chapman, 2018; Strickland et al., 2018; Haxel et al. 2022). A sample of garnet amphibolite (TL25GH-09) intercalated with metachert that represents a fragment of oceanic plate stratigraphy enclosed within the metasedimentary schist at the Gavilan Hills records prograde metamorphic garnet zonation associated with a convex-down zoning profile of Mn from core to rim whereas both Ca and Mg increase over the same interval (supplementary material). Chemical compositions of garnet core and rim in equilibrium with amphibole, plagioclase, quartz, epidote, rutile, ilmenite and titanite, indicate that garnet grew on a clockwise prograde P-T path from 0.7 ± 0.05 GPa and 554 ± 15 °C and to peak P-T conditions of 0.8 ± 0.09 GPa and 592 ± 39 °C. U-Pb zircon geochrobology constrains peak metamorphism between ca. 70-65 Ma (Haxel et al., 2022; Jacobson et al. 2007). In contrast, detrital zircon analysis from these rocks suggest they were deposited at the trench at ca. 73 Ma (Seymour et al. 2018; Jacobson et al. 2007). Since PORS is also exposed in the Plomosa Mts (Strickland et al. 2016;

∼25 km away from the Harcuvar Mountains), the similar peak pressures and overlapping timing of metamorphism of the PORS and the Harcuvar-Harquahala migmatites requires an explanation, which we discuss below.

DISCUSSION

A Case for Channel Flow in Arizona

The new field observations, thermobarometry and geochronology, demonstrate that an inverted metamorphic field gradient occurs across the Hercules, Centennial and Harquahala Thrusts and moving further northeast up structural section across the Harquahala and Harcuvar Mountains. These structures were responsible for overthrusting metamorphosed Proterozoic basement towards the SW onto Cretaceous sediments and Jurassic volcanics. Top-SW shearing likely commenced in the region at ca. 86 Ma as the Tyson Wash granite in the northern Dome Rock Mountains was syn-to-post kinematic with respect to the Tyson-Valenzuela thrust (Boettcher, 1996; Isachsen et al., 1999) and shearing was ongoing on the Hercules, Centennial and Harquahala Thrusts between ca. 76-70 Ma (Fig. 7). In contrast above the thrusts, at higher structural levels, higher grade metamorphic rocks, migmatites and leucogranites are affected by opposite top-NE shearing that pre-dated the Miocene extension as the fabrics are cross-cut by ca. 63-55 Ma undeformed pegmatites and leucogranite dikes (Wong et al. 2023).

Top-NE shearing is associated with normal sense displacement and outcrop fabrics and structures suggest it occurred in the presence of partial melt between ca. 76-63 Ma (Fig. 7). Therefore, both shear zones with opposite kinematics were active at the same time approximately between ca. 76-70 Ma (Fig. 7). The field relations and P-T-t data also require that the thrust responsible for the burial and prograde metamorphism of the gneisses and migmatites within the overthrusted sheets to peak metamorphic pressures of 0.75 GPa (∼28-30 km depth) was not the Hercules, Centennial or Harquahala Thrusts. It must have been a structurally higher thrust that was active earlier and potentially reactivated with top-NE kinematics.

Because the Mesozoic metasedimentary rocks structurally beneath the Hercules Thrusts never achieved pressures greater than ∼0.4 GPa, it requires that the overthrusted sheet of high-grade metamorphic rocks once buried at ∼28-30 km depth (as implied by the metamorphic pressures of 0.75 GPa) was extensively thinned at the same time as overthrusting. If no thinning of the overthrusted sheet occurred, metamorphic pressures in the immediate footwall of the Hercules Thrust should be greater than 0.75 GPa (Fig. 8). Rapid erosion (>2 km/Myr) could potentially explain this data, however one would expect to see a significant amount of detrital metamorphic grains within the McCoy Mountains Formation. Furthermore, rapid erosion alone cannot explain the opposing high temperature kinematic indicators.

Our preferred interpretation to rectify the field observations and P-T-t data is the operation of a syn-orogenic extrusion mechanism (channel flow) that transported weak partially melted mid to lower crust towards the SW (Fig. 9). In this model, the Hercules Thrust associated with top-SW kinematics would define the base of the extruding

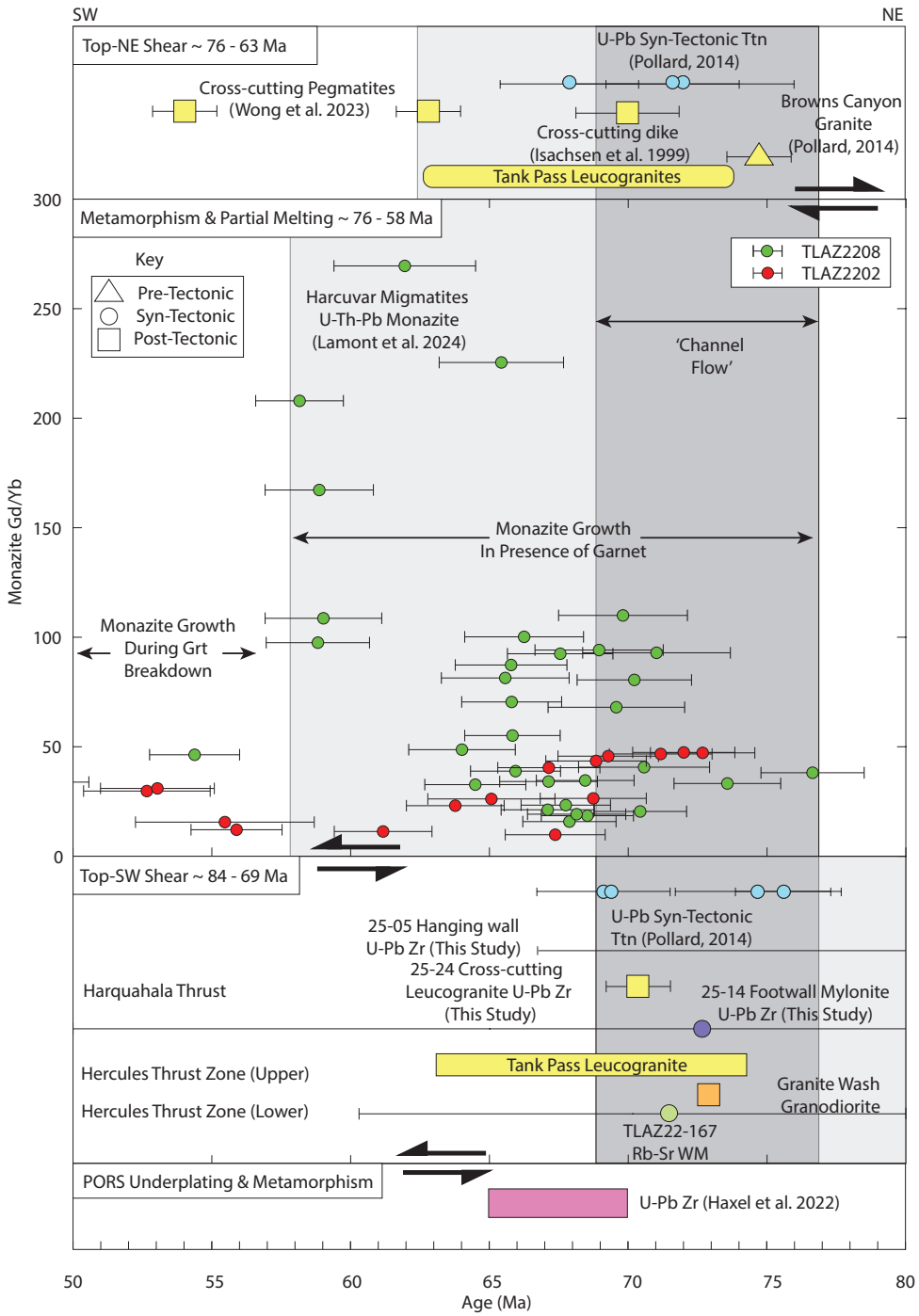

Fig. 7: Time chart showing the overlapping timing constraints for metamorphism and partial melting, top-SW shearing and top-NE shearing

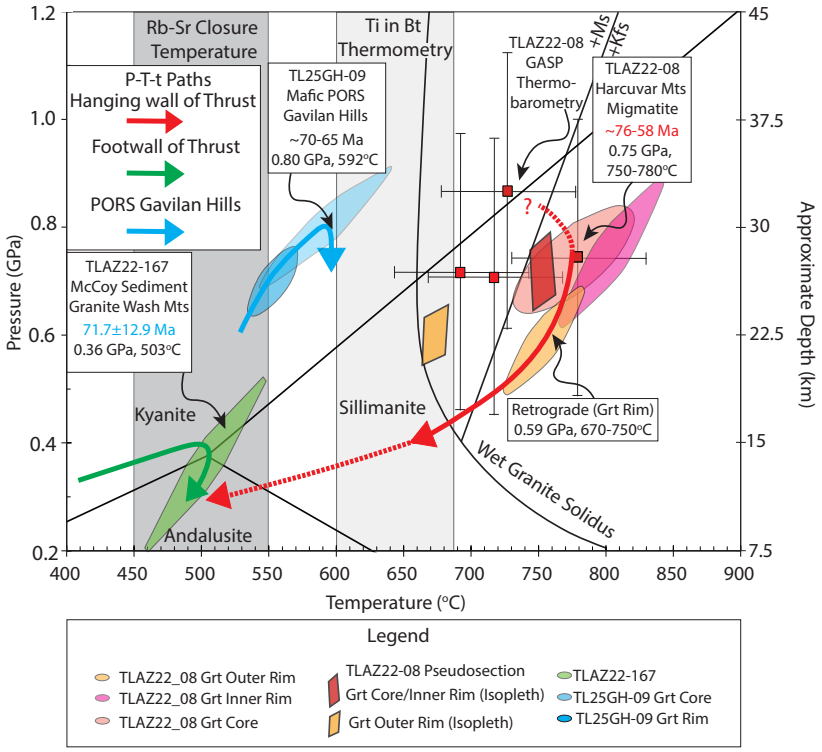

Fig. 8: P-T-t diagrams highlighting the calculated P-T conditions for TLAZ22-167, TLAZ22-08, and TLGH25-09. Note the contrasting P-T loops in the hanging wall and footwall of the Hercules Thrust and the underplated Pelona-Orocopia-Rand-Schists (PORS), integrated with geochronology. Also note the similar peak pressures in the hanging wall migmatites and PORS.

channel or wedge of high-grade metamorphic rocks and migmatites, whereas the top-NE shear zones within the migmatites at higher structural levels would represent a passive roof normal fault defining the top of the channel. Since both top-SW and top-NE shear zones were active simultaneously between ca. 76-70 Ma, syn-orogenic extrusion or channel flow can therefore explain the exhumation of rock from pressures of ca. 0.75-0.36 GPa, without burying the footwall to significant depths.

At approximately this same time interval (ca. 70-65 Ma), the PORS were underplated directly beneath the North American crust and record similar pressures of ca. 0.8 GPa to that of the migmatites within the overthrusted sheets (Fig. 8). The overlapping metamorphic pressures, timing of metamorphism, and proximity of the PORS to the Harcuvar-Harquahala migmatites (∼25 km), therefore potentially creates a space problem if there was no differential movement of mid to lower crustal material (Fig. 9B).

However, volatiles released from dehydration reactions occurring along the low-angle Farallon plate interface likely migrated directly across the Moho and into the

base of the overlying North American crust (Lamont et al. 2024). The addition of slab derived volatiles (e.g. H_2O, CO_2) would act to reduce the solidus of previously dry Proterozoic aged mid to lower crustal rocks and cause significant water-fluxed crustal melting (reaching up to 35% volume locally). This magnitude of partial melting would cause a breakdown in the solid rock framework (Rosenberg & Handy, 2005; Jamieson et al. 2011). This would cause significant rheological weakening, and a viscosity reduction by up to four orders of magnitude (from $\sim 10^{21}$ to $\sim 10^{17}$ PaS), resulting in significant lateral and vertical density contrasts within the North American crust. Additionally, because the Colorado Plateau to the immediate NE of the area remained relatively undeformed during the Sevier-Laramide orogenies and subsequent Cenozoic extension, and maintained >100 km lithospheric thickness (Golos & Fischer, 2022), it likely acted as a rigid backstop, buttressing the Late Cretaceous contractional deformation. It is also possible that the focused contraction caused the lower crust to be initially underthrust beneath the lithospheric wedge at the western margin of the Colorado Plateau. This would be consistent with the thick crust (>50 km) along the Colorado Plateau Transition Zone that is predicted in palispathic restorations (Bahadori et al. 2018). The combination of these processes potentially facilitated ductile extrusion of the mid to lower crust towards the SW. This extrusion mechanism is also consistent with the pulse of uplift along the Colorado Plateau Transition Zone (Kapp et al. 2023), associated with bulldozing the lower crust and subcontinental lithospheric mantle during the onset of low angle subduction (Chapman et al. 2020; Kapp et al. 2023).

Underplating a significant thickness of the PORS, (likely >8 km constrained by seismic reflection investigations beneath the Mojave; Cheadle et al. 1986) also added buoyant felsic meta-sedimentary material to the base of the North American crust in place of lithospheric mantle. This likely caused isostatic uplift and increased gravitational potential energy above the area of underplating and flat slab subduction. However, the area was likely still in an overall contractional setting due to strong coupling along the plate interface, bulldozing the sub-continental lithospheric mantle and end-load at the trench. However, on longer timescales, continued underthrusting of the Farallon flat slab caused cooling and refrigeration of the North American crust (English et al. 2003), consistent with peak metamorphism lasting only $\sim$ 10-15 Myrs and followed by cooling between ca. 60-40 Ma, constrained by Rb-Sr and Ar-Ar cooling ages from the region (Richard et al. 1990; Lamont et al. 2024).

Although the P-T-t data we present and discuss here from the Harcuvar, Harquahala and Granite Wash Mountains is fairly limited, it is consistent with the 1st order predictions of syn-convergent extrusion or channel flow. However, further structural, geochronological and petrological investigations on these rocks will lead to a much greater understanding and rigorously test our proposed model.

Implications for Cordilleran Tectonics

Although the mid to lower crust is rarely exposed across the SW USA in such a complete section, there are numerous magnetite bearing Ms+Grt±Bt peraluminous intrusions that have isotopic and petrological features consistent with water-fluxed melting of Proterozoic crust, as recorded in the Harcuvar-Harquahala migmatites. Water-fluxed crustal melting preferentially consumes plagioclase and K-feldspar which

are the main hosts of Sr in a rock. Therefore, water-fluxed crustal melting would be expected to produce a hydrous, siliceous and oxidized melt that has an elevated Sr/Y ratio. Such magmas are consistent with the petrography and geochemistry of many peraluminous granites across Arizona and the SW USA.

Metaluminous and peraluminous intrusions and porphyry copper deposits get systematically younger across Arizona from NW to SE between ca. 73-45 Ma. From NW-SE the peraluminous intrusions include Diamond Joe (ca. 72 Ma; Chapman et al. 2017), Tank Pass Granite (ca. 75-66 Ma; Isachen et al. 1999; Wong et al. 2023), Vulture Mountains (ca. 68 Ma; Rehrig et al. 1980); White Tank Mountains (ca. 56 Ma; Lamont et al. 2024), Pichacho Mts (ca. 58 Ma), Wilderness Suite Granite (ca. 56-45 Ma; Fornash et al. 2013) in the Catalina-Rincon MCC, Pan Tak granite (58-48 Ma; Chapman et al. 2023) in the Coyote Mts, Texas Canyon (56 Ma; Lamont et al. 2024) in the Dragoon Mountains, and the Renello Suite Granites in the Pinaleño Mountains (ca. 56 Ma; Scoggin et al. 2021). The diachronous timing of these crustal-derived granites implies a mid-crustal zone of water-fluxed partial melting that also systematically gets younger towards the SE during the Late Cretaceous to Paleocene.

Water-fluxed crustal melting in Arizona can be explained by the addition of water derived from metamorphic dehydration reactions that occurred on the Farallon slab infiltrating directly across the Moho, during the onset of low angle subduction, before significant refrigeration occurred (Lamont et al. 2024). Therefore, the southeastward migration of water-fluxed crustal melting likely corresponds to time transgressive Farallon slab-flattening (Lamont et al. 2024).

An additional noteworthy observation is that, upon restoring the Miocene extension, the Harcuvar and Harquahala migmatites dated at ca. 76-60 Ma would project 60 km towards the NE, directly beneath the ca. 72 Ma Bagdad porphyry copper deposit (Barra et al. 2003). Therefore the mid to lower crustal exposures of migmatites and anatectic rocks may represent the deep crustal root zone of the Laramide porphyry copper deposits.

However, there is only relatively local evidence of this ductile extrusion process confined to the MFTB and eastern Mojave Desert. Several Late Cretaceous extensional shear zones are exposed across the Mojave region (Hodges & Walker, 1992; Wells & Hoisch, 2008) which could represent the roof shear zone of an extruding channel. In particular, the Little Piute Mountains, Old Woman Mountains and the Kilbeck Hills in SE California, expose the E-verging Scanalon Thrust and W-verging Meteor Fault, which are parallel structures separated by 1-2 structural km and show opposing kinematics (Howard et al. 1997). These structures have been previously interpreted as forming during a phase of contraction followed by regional extension at ca. 73 Ma (Hodges and Walker, 1992; Wells & Hoisch, 2008). Alternatively, it may be possible that these structures represent the continuation of a westward verging syn-orogenic mid-crustal channel of high-grade metamorphic rock.

However, elsewhere in southern Arizona, where crustal melts and peraluminous granites are exposed, there is only limited evidence for syn-anatectic thrusting. The best example is a thrust fault which mylonitizes the roof of the ca. 56 Ma Texas Canyon Ms+Bt+Grt peraluminous granite in Dragoon Mountains in SE Arizona. Here, the Pinal Schist Proterozoic basement is thrust on top of Cretaceous Bisbee

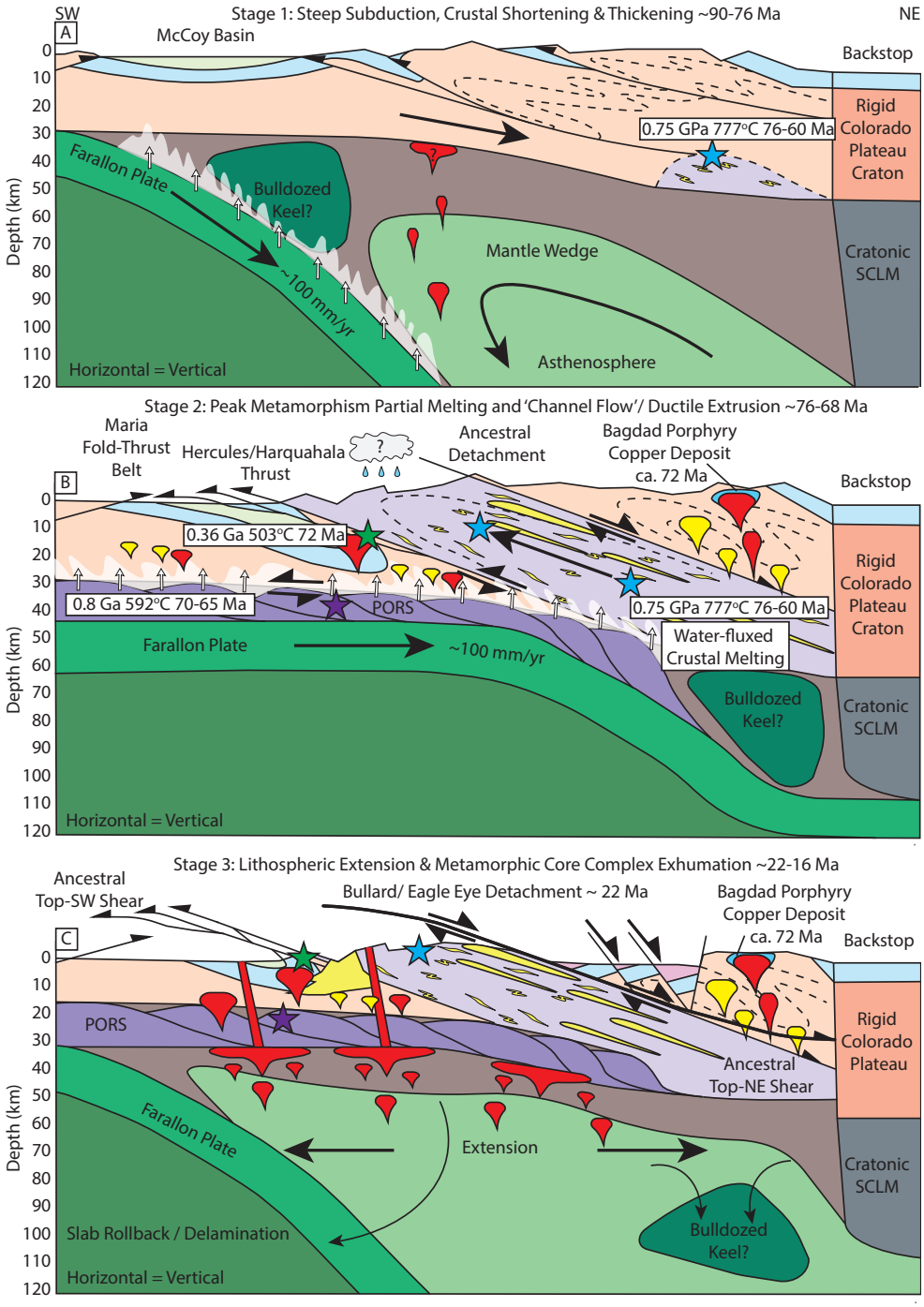

Fig. 9: Channel Flow Model for the Harcuvar-Harquahala-Granite Wash Mountains. A) Stage 1: Contraction and crustal thickening resulting in burial of rocks and heating during steep subduction of the Farallon Plate between ca. 90-76 Ma. B) Stage 2: Onset of low angle subduction resulting in underplating of the PORS at 0.8 GPa, resulting in dehydration reactions liberating fluid and inducing water-fluxed crustal melting and rheological weakening of the mid to lower North American Crust, resulting in ductile extrusion of the mid to lower crust towards the SW, i.e. 'channel flow' between ca. 76-68 Ma forming the ancestral top-SW shear fabrics along the channel base and top-NE shear fabrics along the channel passive roof shear zones. C) Stage 3: Slab delamination and onset of Miocene regional extension forming the Bullard and Eagle Eye Detachments that reactivate and capture the earlier extrusion related shear zones.

Group sediments and the thrust is cut by a Grt+Ms pegmatite dike (personal observation; Keith et al. 2025) suggesting thrusting during the early stages of pluton emplacement. However, the extensive peraluminous crustal derived granites in the Catalina-Rincon MCC, Coyote, Pinaleño Mountains do not appear to be bound by thrust faults, and the timing of thrusting in these areas is interpreted to be 75-65 Ma (e.g. Favorito & Seedorf, 2024), which is ∼10-15 million years before the emplacement of the peraluminous anatectic rocks. The ductile extrusion feature we document in the Harcuvar-Harquahala-Granite Wash mountains is therefore unlikely to be an orogen wide structure.

Finally, our proposed syn-orogenic extrusion mechanism during the underplating and accretion of the PORS could explain the paradoxical geochemical and metamorphic evidence for thick crust across Arizona during the Late Cretaceous-Paleocene (Chapman et al. 2020; Lamont et al. 2024) and the relatively scarce evidence for upper-crustal shortening features as the crust was thickened from primarily underplating. Syn-orogenic extrusion may also facilitate the localization of extensional strain and final MCC exhumation in the same location during delamination of a low angle slab at a later time.

Comparison with the Himalaya and East Greenland Caledonides

Closer inspection of the Harcuvar-Harquahala-Granite Wash Mountains reveals many similarities, and a few key differences with the Greater Himalayan Series (GHS) and the retro-wedge of the East Greenland Caledonides (EGC) (Fig. 10).

All three locations show inverted metamorphic isograds along the basal thrust fault (Main Central Thrust at the base of the GHS, a thrust fault separating the foreland and 'infrastructure' in the EGC, and the Hercules/Harquahala Thrusts at the base of the Harcuvar-Harquahala migmatites in Arizona; Fig. 10). These inverted isograds can be spatially linked with right-way up metamorphic isograds associated with opposing normal sensed shear at higher structural levels along the channel ('infrastructure') roof (Searle and Rex, 1989, Hodges, 2016). Thermobarometric data support this interpretation, as P-T conditions increase up-section above he Hercules and Harquahala Thrusts in the Harcuvar, Harquahala and Granite Wash Mountains from greenschist to upper amphibolite facies (0.36 Ga and 503°C to 0.75 GPa and 777°C), similar to structurally above the Main Central Thrust in the Himalaya and above the base of the EGC 'infrastructure' (White and Hodges, 2002), although in some places the thrust has been reactivated as an extensional detachment (Hodges, 2016). In contrast, supra-solidus deformation is overprinted by sub-solidus deformation beneath the South Tibetan Detachment (STD), Fjord Region Detachment (FRD) and the Late Cretaceous-Paleocene syn-migmatitic mylonites in the Harcuvar-Harquahala Mountains. The highest-grade rocks therefore appear close to the center to upper half of the GHS, EGC 'infrastructure' and the Harcuvar-Harquahala MCCs.

Leucogranites are also abundant in all three settings and are spatially related to a widespread sillimanite-bearing migmatite zone and consist of multiple phases of intrusions spanning ∼10 Myrs (Searle et al. 2010; Wong et al. 2023). The

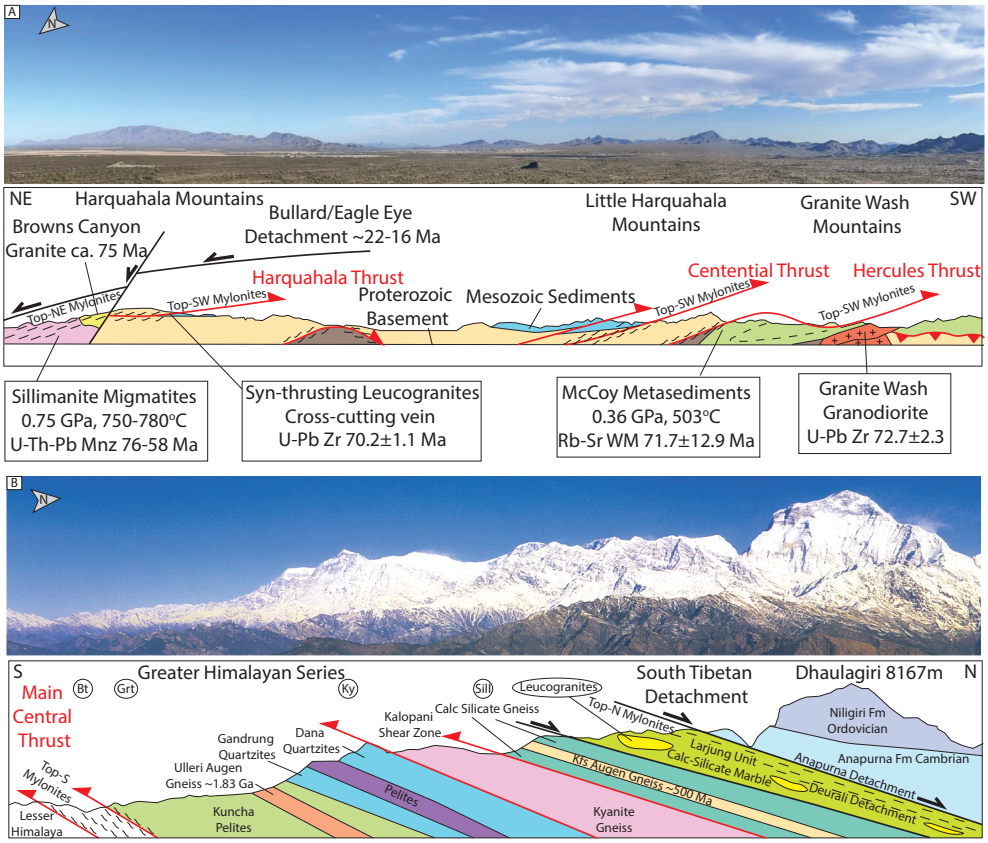

Fig. 10: Comparison between the field relationships and metamorphism in A) the Harcuvar-Harquahala-Granite Wash Mountains and B) the Greater Himalayan series in the high Himalaya adapted from Searle, (2010).

leucogranites in the Himalaya and Arizona have the composition quartz–K-feldspar–plagioclase–muscovite–tourmaline–biotite–garnet, with some later intrusions containing magmatic cordierite (altered to pinite) and/or andalusite. The leucogranites are also highly peraluminous (molar A/CNK $>$ 1.1), contain high boron concentrations (abundant tourmaline), and elevated $^{87}Sr/^{86}Sr$ ratios, indicating a purely crustal melting origin (Harris & Massey 1994; Hopkinson et al. 2020; Lamont et al. 2024).

However, the ca. 74-64 Ma Tank Pass leucogranite in the Harcuvar and Granite Wash Mountains cross-cut top-SW shear fabrics, whereas ca. 70-55 Ma pegmatitic dikes cross-cut top-NE shear fabrics. This is somewhat similar to the anatectic granites of the infrastructure in EGC (Hodges et al. 2016), where unfoliated late-stage anatectic melts cut FRD fabrics and in some cases intrude across the FRD and into the overlying 'superstructure', effectively constraining the age of the FRD to ca. 425 Ma (White et al. 2002).

U–(Th)–Pb monazite dating shows that peak metamorphism and melting in the GHS evolved from late Eocene–Oligocene kyanite-grade metamorphism to lower pressure and higher temperature sillimanite-grade metamorphism. During the later stages cordierite formed at pressures <0.5 GPa. Kyanite grade partial melting is represented by small, plagioclase-poor, kyanite+quartz-bearing leucosomes within the GHS gneisses. These melts formed at $\sim$ 720–710°C and ca. 1.0 GPa by water-fluxed melting between ca. 40-30 Ma (Laccarino et al. 2015). However, most GHS leucogranites were formed by muscovite or biotite dehydration reactions due to decompression between ca. 25-15 Ma (Cottle et al. 2009, 2015). Mid-crustal melting during the early to mid-Miocene likely triggered the large-scale ductile flow of a partially molten layer of mid-crust bounded by the MCT ductile shear zone below and the STD ductile shear zone and low-angle normal faults above.

Within the the EGC 'infrastructure', metamorphic conditions reached upper amphibolite to granulite facies with extensive partial melting during Caledonian deformation (ca. 440-405 Ma) which overlaps with the timing of normal sensed shearing on the roof shear zone (ca. 440-425 Ma) (Andresen et al. 2007; Elvevold et al. 2003; Gilotti & McClelland 2005; Hartz et al. 2000, 2001; Kalsbeek et al. 2001; Strachan & Martin 2001; Watt et al. 2000; White & Hodges 2003; White et al. 2002).

Migmatites from the Harcuvar Mountains give U–(Th)–Pb monazite dates spanning ca. 76-58 Ma (Walsh et al. 2016; Lamont et al. 2024) that represent the timing of peak metamorphism and crustal anatexis that overlap with the timing of top-SW thrusting (ca. 86-70 Ma) and top-NE shearing (ca. 76-63 Ma). The migmatites also record a similar P-T path to the GHS with kyanite overprinted by sillimanite associated with decompression and partial exhumation. However, Harcuvar-Harquahala migmatites have very extensive leucosome components locally comprising >30-35% of the rock volume, and they have trondhjemitic (plagioclase-quartz) compositions. There is also minimal peritectic K-feldspar yet abundant muscovite in partially melted Proterozoic gneisses. Together, these features suggest that partial melting occurred by the addition of water, which preferentially consumed plagioclase during anatexis (Lamont et al. 2024), rather than incongruent melting of muscovite or biotite (Weinberg and Hasalova, 2015). Since plagioclase is the main host of Sr, water-fluxed crustal melting can potentially explain the high Sr/Y ratios that characterize the Late-Cretaceous-Paleocene peraluminous granites across Arizona and the SW USA (Chapman et al. 2020).

However, water-fluxed crustal melting requires an external source of water. In Arizona, this was likely derived from dehydration reactions occurring within the upper part of the low angle Farallon slab, based on the overlapping timing of metamorphism (ca. 70-65 Ma) recorded by the PORS. In contrast, the age of PORS underplating, water-fluxed crustal melting, and peraluminous granite intrusion is older to the west in the Mojave Desert, implying that the locus of slab dehydration and water-fluxed crustal melting was time transgressive and was followed by refrigeration due to progressive underplating. In contrast, the deep crustal earthquakes within the Indian shield underthrusting beneath the Himalaya suggest it consists of dry granulites that have been previously dehydrated (Priestley et al. 2008), and therefore an unlikely

source of water. As such, most Himalayan migmatites and leucogranites formed by the incongruent breakdown of muscovite (e.g. Patiño Douce & Harris, 1998).

The Harcuvar-Harquahala-Granite Wash Mountains and the EGC retro-wedge also show along strike variation in metamorphic grade, and diachronous timing of thrusting and ductile flow within the mid to lower crustal channel ('infrastructure') (Hodges, 2016), which contrasts with the Himalaya. Both settings are also affected by post-orogenic regional extension (McClay, 1986), that in some cases reactivates the earlier shear zones (Hodges, 2016). In Arizona, regional extension occurred at ca. 22-16 Ma, whereas within the EGC it occurred at ca. 350-360 Ma. In both settings, regional extension commenced some ca. 40-50 Myrs after a phase of syn-convergent extrusion.

In summary, all three locations show a similar overall trans-lithospheric orogenic structure separated by key decoupling horizons (Hodges, 2016): 1) An 'extensional' decoupling horizon representing the strain discontinuity existing between the upper crustal 'superstructure' and mid to lower crustal 'infrastructure', associated with excision of crust through large-displacement normal faulting. Although this decoupling horizon may be referred to as an extensional fault because of the kinematics, it does not indicate extension on the scale of the entire crust because the upper crustal extension is compensated for by contractional deformation at deeper structural levels (Hodges, 2016). 2) The base of the channel or 'infrastructure' represents large-displacement thrust faults, as it marks the discontinuity between the weak, mobilized mid to lower crustal metamorphic rocks and the stronger rocks of the orogenic allochthonous foreland which are associated with a fold and thrust belt (Boyer & Elliott, 1982). 3) Beneath the allochtonous foreland, the sole fault separates the orogenic wedge from the underthrusted substrate that experiences little internal deformation (Hodges, 2016). In the Himalaya and East Greenland Caledonides, dry cratonic continental lithosphere was underthrust beneath the orogenic wedge, whereas in Arizona, the Farallon Slab of oceanic affinity was underthrust at a low angle beneath North America and therefore the sole thrust of the orogenic wedge would have localized along the plate interface.

CONCLUSIONS

We document an inverted metamorphic gradient across the Harcuvar-Harquahala-Granite Wash Mountains which is characteristic of hotter and deeper rocks being thrust on top of colder and shallower rocks. This is further supported by the overlapping timing of top-SW thrusting on the Hercules and Harquahala Thrusts with top-NE shearing affecting higher-grade metamorphic rocks and migmatites at higher structural levels. These features are consistent with ductile extrusion or channel flow of mid to lower crustal high-grade metamorphic rock, gneisses and migmatites towards the SW. Southwestward directed flow was likely facilitated by water-fluxed crustal melting and associated rheological weakening of the mid to lower crust. This likely occurred due to the addition of slab-derived volatiles infiltrating across the Moho during low angle subduction of the Farallon slab directly beneath North America.

We therefore propose that the 'ancestral' top-NE shear fabrics preserved within the Harcuvar-Harquahala-Granite Wash Mountains do not represent crustal extension or 'orogenic collapse' but rather the roof shear zone of a mid to lower crustal

channel or extruding wedge in an overall contractional setting. This ductile extrusion occurred more than ∼40 Myrs before regional Cenozoic extension responsible for final MCC exhumation associated with the brittle-ductile Bullard/Eagle Eye Detachments at ca. 22-16 Ma, that potentially reactivated the earlier roof shear zone of this mid to lower crustal channel or wedge (Fig. 9C). Therefore, the Harcuvar-Harquahala-Granite Wash Mountains record pre-extensional orogenic events that have been overprinted or captured by a completely unrelated normal fault (Bullard/ Eagle Eye Detachment) during a more recent phase of regional extension. We therefore suggest that metamorphic rocks and ductile shear zones exposed within the footwalls of MCCs around the world, especially in cases where 'extensional' fabrics may predate recognized regional extension, be carefully re-examined in light of these new data.

Supplementary Information. Supplementary Material is available using the following link:

Acknowledgments. This work benefited from numerous discussions with Adam Gorecki, Frances Cooper and particularly Mike Searle. TL thanks Matt Loader, Noah Metz and Joel Leonard for assistance in the field upon first visiting the area during 2021-2022. TL thanks Steve Reynolds for an overview discussion of the Harcuvar-Harquahala Mountains and targeted sampling areas for further research. Gordon Haxel and Carl Jacobson are thanked for thought provoking discussion and pointing TL and GE to investigate the PORS at the Gavilan Hills. SS acknowledges analytical assistance from Charles Knaack (WSU RIGL), and funding assistance from NSF-EAR2342159 awarded to JH.

Declarations

- Funding: SS acknowledges analytical assistance from Charles Knaack (WSU RIGL), and funding assistance from NSF-EAR2342159 awarded to JH.
- Competing interests: The authors declare that there is no competing financial interests.
- Ethics approval: Not Applicable
- Consent to participate: Not Applicable
- Consent to publication: Not Applicable
- Availability of data and materials: Full data and materials are presented in the online Supplementary Material.
- Code availability: The codes used for petrological modelling are available at: https://hpxeosandthermocalc.org/the-thermocalc-software/
- Authors' contributions: TL conceived the idea and wrote the first draft. All authors conducted fieldwork and sample collection. SS conducted the U-Pb analyses and TL collected the EPMA data and conducted the thermobarometric calculations. All authors contributed to subsequent drafts.

MATERIALS AND METHODS

Electron Probe Micro-Analysis (EPMA)

The compositions of phases in samples TLAZ22-08 and TLAZ22-167 were presented in Lamont et al. (2024). Additional electron probe micro-analysis (EPMA) were performed on sample TL25GH-09 using a CAMECA SX5-FE electron microprobe at the Department of Earth Sciences, University of Oxford. Operating conditions involved an accelerating voltage of 15.0 keV corresponding to a current of 20 nA, a range of primary standards were used, including andradite (Fe, Mg, Ca), TiO_2 (Ti), Mn metal (Mn), labradorite (Na, Al, Si) and sanidine (K) for major elements, and secondary standards include diopside, KK1, SPH Labradorite, RN18 and FDLA1. Garnet line profiles were collected using a 75-100 μm step size across all garnets from rim to rim, equating to $\pm$ 30-50 analyses per garnet. The full results are presented in supplementary table S1 and the garnet line chemical profiles are presented in the supplementary material.

Thermobarometry

P-T calculations on samples TLAZ22-08 and TLAZ22-167 were presented in Lamont et al. (2024). Additional calculations were performed on sample TL25GH-09, a garnet amphibolite from the Orocopia Schist at the Gavilan Hills, SE CA, using Average P-T mode in THERMOCALC version TC-3.40i (Powell and Holland, 1988, 1994) using dataset 62 (Holland & Powell, 2011) with characteristic end members judged to be in textural equilibrium. Activities of phase end-member were calculated using the average phase compositions and garnet core and garnet rim compositions determined by EPMA and running through the program AX62 (last accessed April 2026). The complete results are presented in Supplementary table S2.

U–Th–Pb Geochronology

Zircon U-Pb isotope measurement at Washington Sate University were performed with a Thermo Element2 HR-ICP-MS connected to a Teledyne Photon Machines Analyte Excite 193 nm ArF laser ablation system. Reference materials were analyzed during the session and typically bracketed every $\pm$10 unknown analyses. FC-1 (1099 Ma; Paces & Miller, 1993) and Plešovice (337.1 Ma; Sláma et al., 2008) standards were used as principal reference materials to correct for $^{207}Pb/^{206}Pb$ and $^{206}Pb/^{238}U$, respectively. Secondary reference materials including 91500 (1065 Ma; Wiedenbeck et al., 1995) were used to evaluate the accuracy of the analyses during each session. The U-Pb isotope data and downhole fractionation corrections were reduced in Iolite v4 (Paton et al., 2010, 2011). The U-Pb ages obtained for each zircon standard in different analytical sessions are within $\pm$1 % of their reported "true" age. The full results and concordia plots and are presented in the supplementary material and supplementary table S3.

References

Andresen A, Hartz EH, Vold J. (1998). A late orogenic extensional origin for

690 the infracrustal gneiss domes of the East Greenland Caledonides (72–74◦N).
691 Tectonophysics, 285, 353–69
692 Bahadori, A., Holt, W. E., & Rasbury, E. T. (2018). Reconstruction modeling of
693 crustal thickness and paleotopography of western North America since 36 Ma.
694 Geosphere, 14(3), 1207-1231.
695 Barra, F., Ruiz, J., Mathur, R., & Titley, S. (2003). A Re–Os study of sulfide minerals
696 from the Bagdad porphyry Cu–Mo deposit, northern Arizona, USA. Mineralium
697 Deposita, 38(5), 585-596.
698 Barth, A.P., Wooden J.K., Jacobson C.E., & Probst K., (2004). U-Pb geochronology
699 and geochemistry of the McCoy Mountains Formation, southeastern California: A
700 Cretaceous retroarc foreland basin: Geological Society of America Bulletin, 116,
701 142– 153, doi: 10.1130/B25288.1.
702 Beaumont, C., Jamieson, R. A., Nguyen, M. H., & Lee, B. (2001). Himalayan tectonics
703 explained by extrusion of a low-viscosity crustal channel coupled to focused surface
704 denudation. Nature, 414(6865), 738-742.
705 Boyer, S. E., & Elliott, D. (1982). Thrust systems. AAPG Bulletin 66, 1196–1230.
706 https://doi.org/10.1306/03B5A77D-16D1-11D7-8645000102C1865D
707 Bryant, B., & Wooden, J. L. (2008). Geology of the northern part of the Harcuvar
708 complex, west-central Arizona (52). US Geological Survey.
709 Burchfiel, B. C., & Royden, L. H., (1985). North-south extension within the convergent
710 Himalayan region: Geology, 13, 679-682.
711 Burchfiel, B. C., Zhiliang, C., Hodges, K. V., Yuping, L., Royden, L. H., Changrong,
712 D., & Jiene, X. (1992). The South Tibetan detachment system, Himalayan oro-
713 gen: Extension contemporaneous with and parallel to shortening in a collisional
714 mountain belt.
715 Caby, R. (1983). Le grand chevauchement central himalayaen: Nouvelles donnees sur
716 le metamorphicsme inverse a la base de la Dalle du Tibet. Revue de geologie
717 dynamique et de geographie physique, 24, 89-100.
718 Caylor, E. A., Carrapa, B., DeCelles, P. G., & Gehrels, G. E. (2024). The real McCoy:
719 A record of deep-water basin deposition in southwestern North America during
720 the Cretaceous. Basin Research, 36(5), e12902.
721 Chapman, A. D. (2017). The Pelona–Orocopia–Rand and related schists of southern
722 California: A review of the best-known archive of shallow subduction on the planet.
723 International Geology Review, 59(5-6), 664-701.
724 Chapman, A. D., Rautela, O., Shields, J., Ducea, M. N., & Saleeby, J. (2020). Fate
725 of the lower lithosphere during shallow-angle subduction: The Laramide example.
726 GSA Today, 30(1), 4-10.
727 Chapman, J. B., Greig, R., & Haxel, G. B. (2020). Geochemical evidence for an oro-
728 genic plateau in the southern US and northern Mexican Cordillera during the
729 Laramide orogeny. Geology, 48(2), 164-168.
730 Chapman, J. B., Dafov, M. N., Gehrels, G., Ducea, M. N., Valley, J. W., & Ishida, A.
731 (2018). Lithospheric architecture and tectonic evolution of the southwestern US
732 Cordillera: Constraints from zircon Hf and O isotopic data. Geological Society of
733 America Bulletin, 130(11-12), 2031-2046.
734 Chapman, J. B., Pridmore, C., Chamberlain, K., Haxel, G., & Ducea, M. (2023).

Himalayan-like crustal melting and differentiation in the southern North American Cordilleran anatectic belt during the Laramide orogeny: Coyote Mountains, Arizona. Journal of Petrology, 64(10), egad075.

Cheadle, M. J., B. L.Czuchra, T.Byrne, C. J.Ando, J. E.Oliver, L. D.Brown, S.Kaufman, P. E.Malin, and R. A.Phinney (1986), The deep crustal structure of the Mojave Desert, California, from Cocorp seismic reflection data, Tectonics, 5(2), 293–320, doi:10.1029/TC005i002p00293.

Cottle, J. M., Jessup, M. J., Newell, D. L., Searle, M. P., Law, R. D., & Horstwood, M. S. (2007). Structural insights into the early stages of exhumation along an orogen-scale detachment: The South Tibetan Detachment System, Dzakaa Chu section, Eastern Himalaya. Journal of Structural Geology, 29(11), 1781-1797.

Cottle, J. M., Jessup, M. J., Newell, D. L., Horstwood, M. S., Noble, S. R., Parrish, R. R., ... & Searle, M. P. (2009). Geochronology of granulitized eclogite from the Ama Drime Massif: Implications for the tectonic evolution of the South Tibetan Himalaya. Tectonics, 28(1).

Cottle, J. M., Searle, M. P., Jessup, M. J., Crowley, J. L., & Law, R. D. (2015). Rongbuk re-visited: Geochronology of leucogranites in the footwall of the South Tibetan detachment system, Everest region, southern Tibet. Lithos, 227, 94-106.

Dalmayrac, B., & Molnar, P. (1981). Parallel thrust and normal faulting in Peru and constraints on the state of stress. Earth and Planetary Science Letters, 55(3), 473-481.

Dewey, J. F. (1988). Extensional collapse of orogens. Tectonics, 7(6), 1123-1139.

Dyck, B., Waters, D. J., St-Onge, M. R., & Searle, M. P. (2020). Muscovite dehydration melting: Reaction mechanisms, microstructures, and implications for anatexis. Journal of Metamorphic Geology, 38(1), 29-52.

Elvevold, S., Thrane, K., Gilotti, J., A. (2003). Metamorphic history of high-pressure granulites in Payer Land, Greenland Caledonides. Journal of Metamorphic Geology. 21, 49–63.

England, P. C., and Holland, T.J., (1979). Archimedes and the Tauern eclogites: the role of buoyancy in the preservation of exotic eclogite blocks, Earth and Planetary Science Letters, 44, 2, 287-294, DOI : 10.1016/0012-821X(79)90177-8

English, J. M., Johnston, S. T., & Wang, K. (2003). Thermal modelling of the Laramide orogeny: testing the flat-slab subduction hypothesis. Earth and Planetary Science Letters, 214(3-4), 619-632.

Favorito, D. A., & Seedorff, E. (2024). Temporal and spatial relations between porphyry copper deposits and crustal shortening: Insights from the Laramide arc of Arizona and New Mexico. Economic Geology, 119(6), 1261-1288.

Fornash, K. F., Patchett, P. J., Gehrels, G. E., & Spencer, J. E. (2013). Evolution of granitoids in the Catalina metamorphic core complex, southeastern Arizona: U–Pb, Nd, and Hf isotopic constraints. Contributions to Mineralogy and Petrology, 165(6), 1295-1310.

Gerya, T. V., Stöckhert, B., & Perchuk, A. L. (2002). Exhumation of high-pressure metamorphic rocks in a subduction channel: A numerical simulation, Tectonics, 21(6), 1056, doi:10.1029/2002TC001406

Gilotti, J., A., McClelland, W. C., (2005). Leucogranites and the time of extension in

780 the East Greenland Caledonides. Journal of Metamorphic Geology. 113, 399–417.
781 Gilotti J. A., Jones, K. A., & Elvevold, S. (2008). Caledonian metamorphic patterns
782 in Greenland. Geological Society America Memoirs 202, 201–25.
783 Godin, L., Grujic, D., Law, R. D., & Searle, M. P. (2006). Channel flow, ductile extru-
784 sion and exhumation in continental collision zones: An introduction. In R. D. Law,
785 M. P. Searle, & L. Godin (Eds.), Channel flow, ductile extrusion and exhumation
786 in continental collision zones (268, 1–23). Geological Society of London.
787 Golos, E. M., & Fischer, K. M. (2022). New insights into lithospheric structure and
788 melting beneath the Colorado Plateau. Geochemistry, Geophysics, Geosystems,
789 23(3), e2021GC010252. doi.org
790 Grujic, D., Casey, M., Davidson, C., Hollister, L. S., Kündig, R., Pavlis, T., & Schmid,
791 S. (1996). Ductile extrusion of the Higher Himalayan Crystalline in Bhutan:
792 evidence from quartz microfabrics. Tectonophysics, 260(1-3), 21-43.
793 Harris, N., & Massey, J. (1994). Decompression and anatexis of Himalayan metapelites.
794 Tectonics, 13(6), 1537-1546.
795 Hartz, E., & Andresen, A. (1995). Caledonian sole thrust of central East Greenland:
796 a crustal-scale Devonian extensional detachment? Geology 23, 637–40
797 Hartz, E. H., Andresen, A., Hodges K. V., & Martin M. W., (2001). Syncontractional
798 extension and exhumation of deep crustal rocks in the east Greenland Caledonides.
799 Tectonics 20, 58–77
800 Hartz E. H., Andresen A., Martin M. W., & Hodges K. V. (2000). U-Pb and 40Ar/39Ar
801 constraints on the Fjord Region detachment zone: a long-lived extensional fault in
802 the East Greenland Caledonides. Journal of the Geological Society London, 157,
803 795–809.
804 Hodges, K. V. (2016). Crustal decoupling in collisional orogenesis: examples from
805 the East Greenland Caledonides and Himalaya. Annual Review of Earth and
806 Planetary Sciences, 44, 685-708.
807 Hodges, K. V., & Walker, J. D. (1992). Extension in the Cretaceous Sevier orogen,
808 North American Cordillera. Geological Society of America Bulletin, 104(5), 560-
809 569.
810 Holland, T. J. B. & Powell, R. (2011). An improved and extended internally consis-
811 tent thermodynamic dataset for phases of petrological interest, involving a new
812 equation of state for solids. Journal of Metamorphic Geology, 29(3), 333-383.
813 Hopkinson, T., Harris, N., Roberts, N. M., Warren, C. J., Hammond, S., Spencer, C.
814 J., & Parrish, R. R. (2020). Evolution of the melt source during protracted crustal
815 anatexis: An example from the Bhutan Himalaya. Geology, 48(1), 87-91.
816 Howard, K. A., Dennis, M. L., Karlstrom, K., & Phelps, G. A. (1997). Preliminary
817 geologic map of the Little Piute Mountains, California: A digital database (No.
818 97-693). US Geological Survey.
819 Hubbard, M. S. (1989). Thermobarometric constraints on the thermal history of the
820 Main Central Thrust Zone and Tibetan Slab, eastern Nepal Himalaya. Journal of
821 Metamorphic Geology, 7(1), 19-30.
822 Isachsen, C. E., Gehrels, G. E., Riggs, N. R., Spencer, J. E., Ferguson, C. A., Skotnicki,
823 S. J., & Richard, S. M. (1999). U-Pb geochronologic data from zircons from eleven

granitic rocks in central and western Arizona. Arizona Geological Survey Open-File Report 99-5, 27.

Jacobson, C. E., Grove, M., Vucic, A., Pedrick, J. N., & Ebert, K. A. (2007). Exhumation of the Orocopia Schist and associated rocks of southeastern California: Relative roles of erosion, synsubduction tectonic denudation, and middle Cenozoic extension. In Cloos, M., Carlson, W.D., Gilbert, M.C., Liou, J.G., & Sorensen, S.S., eds., Convergent Margin Terranes and Associated Regions: A Tribute to W.G. Ernst: Geological Society of America Special Paper 419, p. 1–37, doi: 10.1130/2007.2419(01).

Jamieson, R. A., Unsworth, M. J., Harris, N. B., Rosenberg, C. L., & Schulmann, K. (2011). Crustal melting and the flow of mountains. Elements, 7(4), 253-260.

Johnston, S., M., & Kylander-Clark, A., R., C., (2013). Discovery of an Eo-Meso-Neoarchean terrane in the East Greenland Caledonides. Precambrian Research, 235, 295–302.

Kalsbeek, F., Jepsen, H. F., & Nutman, A. P., (2001). From source migmatites to plutons: tracking the origin of ca. 435 Ma S-type granites in the East Greenland Caledonian orogen. Lithos 57, 1–21.

Kapp, P., Jepson, G., Carrapa, B., Schaen, A. J., He, J. J. Y., & Wang, J. W. (2023). Laramide bulldozing of lithosphere beneath the Arizona transition zone, southwestern United States. Geology, 51(10), 952–956. https://doi.org/10.1130/G51194.1

Keith, S., C. Rasmussen, J., & Spieth, V. (2026). A New Class of Nonvolcanic, Large, Peraluminous Copper-Oxide Greisen Deposits in Arizona, USA. In Latest Advances in Volcanology. IntechOpen. https://doi.org/10.5772/intechopen.1014159

Klemperer, S. L. (2006). Crustal flow in Tibet: geophysical evidence for the physical state of Tibetan lithosphere, and inferred patterns of active flow. In R. D. Law, M. P. Searle, & L. Godin (Eds.), Channel flow, ductile extrusion and exhumation in continental collision zones (Special Publications, 268, 281–308). Geological Society of London.

Knapp, J. H., and Heizler, M. T., (1987), Thermal History of Crystalline Nappes of the Maria Fold and Thrust Belt, West Central Arizona, Jounral of Geophysical Research, 95, no. B12, 20049-20073.

Laccarino, S., Montomoli, C., Carosi, R., Massonne, H. J., Langone, A., & Visonà, D. (2015). Pressure–temperature–time–deformation path of kyanite-bearing migmatitic paragneiss in the Kali Gandaki valley (Central Nepal): Investigation of Late Eocene–Early Oligocene melting processes. Lithos, 231, 103-121.

Lamont, T. N., Searle, M. P., Waters, D. J., Roberts, N. M., Palin, R. M., Smye, A., ... & St-Onge, M. R. (2020a). Compressional origin of the Naxos metamorphic core complex, Greece: Structure, petrography, and thermobarometry. Geological Society of America Bulletin, 132(1-2), 149-197.

Lamont, T. N., Searle, M. P., Gopon, P., Roberts, N. M., Wade, J., Palin, R. M., & Waters, D. J. (2020b). The Cycladic Blueschist Unit on Tinos, Greece: Cold NE subduction and SW directed extrusion of the Cycladic continental margin under

the Tsiknias Ophiolite. Tectonics, 39(9), e2019TC005890.
Lamont, T. N., Smye, A. J., Roberts, N. M., Searle, M. P., Waters, D. J., & White, R. W. (2023a). Constraints on the thermal evolution of metamorphic core complexes from the timing of high-pressure metamorphism on Naxos, Greece. Geological Society of America Bulletin, 135(11-12), 2767-2796.
Lamont, T. N., Roberts, N. M., Searle, M. P., Gardiner, N. J., Gopon, P., Hsieh, Y. T., ... & White, R. W. (2023b). Contemporaneous crust-derived I-and S-type granite magmatism and normal faulting on Tinos, Delos, and Naxos, Greece: Constraints on Aegean orogenic collapse. Geological Society of America Bulletin, 135(11-12), 2797-2829.
Lamont, T. N., Loader, M. A., Roberts, N. M., Cooper, F. J., Wilkinson, J. J., Bevan, D., ... & Tapster, S. (2024). Porphyry copper formation driven by water-fluxed crustal melting during flat-slab subduction. Nature Geoscience, 17(12), 1306-1315.
Laubach, S. E., Reynolds, S. J., Spencer, J. E., & Marshak, S. (1989). Progressive deformation and superposed fabrics related to Cretaceous crustal underthrusting in western Arizona, USA. Journal of Structural Geology, 11(6), 735-749.
Law, R. D., Searle, M. P., & Simpson, R. L. (2004). Strain, deformation temperatures and vorticity of flow at the top of the Greater Himalayan Slab, Everest Massif, Tibet. Journal of the Geological Society, 161(2), 305-320.
Law, R. D., Jessup, M. J., Searle, M. P., Francsis, M. K., Waters, D. J., & Cottle, J. M. (2011). Telescoping of isotherms beneath the South Tibetan detachment system, Mount Everest Massif. Journal of Structural Geology, 33(11), 1569-1594.
McClay KR, Norton MG, Coney P, & Davis GH. (1986). Collapse of the Caledonian orogen and the Old Red Sandstone. Nature, 323, 147–49.
Means, W.D. (1989). Stretching faults. Geology, 17, 893-896.
Paces, J. B., & Miller, J. D., Jr. (1993). Precise U-Pb ages of Duluth Complex and related mafic intrusions, northeastern Minnesota: Geochronological insights into physical, chemical, and tectonic controls on midcontinent rift magmatism. Journal of Geophysical Research: Solid Earth, 98(B8), 13997-14013.
Patiño Douce, A.E., and Harris, N., (1998), Experimental constraints on Himalayan Anatexis: Journal of Petrology , 39, 689–710, https://doi.org/10.1093/petroj/39.4.689.
Paton, C., Woodhead, J. D., Hellstrom, J. C., Hergt, J. M., Greig, A., & Maas, R. (2010). Improved laser ablation U-Pb zircon geochronology through robust downhole fractionation correction. Geochemistry, Geophysics, Geosystems, 11(3).
Paton, C., Hellstrom, J., Paul, B., Woodhead, J., & Hergt, J. (2011). Iolite: Freeware for the visualisation and processing of mass spectrometric data. Journal of Analytical Atomic Spectrometry, 26(12), 2508-2518.
Platt, J. P., Behr, W. M., & Cooper, F. J. (2015). Metamorphic core complexes: Windows into the mechanics and rheology of the crust. Journal of the Geological Society, 172(1), 9-27.
Powell, R, & Holland, TJB, (1988). An internally consistent thermodynamic dataset with uncertainties and correlations: 3: application methods, worked examples and a computer program. Journal of Metamorphic Geology, 6, 173-204.
Powell, R, & Holland, TJB, (1994). Optimal geothermometry and geobarometry.

American Mineralogist, 79, 120-133.
Priestley, K., Jackson, J., & McKenzie, D. (2008). Lithospheric structure and deep earthquakes beneath India, the Himalaya and southern Tibet. Geophysical Journal International, 172(1), 345–362.
Rehrig W, Shafiqullah M, Damon P, (1980). Geochronology, geology and listric normal faulting of the Vulture Mountains, Maricopa County, Arizona. In: Jenney J, Stone C, editors. Studies in Western Arizona. Tucson: Arizona Geological Society Digest; 1980. 12. 89–110.
Reynolds, S. J., & Spencer, J. E. (1985). Evidence for large-scale transport on the Bullard detachment fault, west-central Arizona. Geology, 13(5), 353-356.
Reynolds, S. J., & Lister, G. S. (1990). Folding of mylonitic zones in Cordilleran metamorphic core complexes: Evidence from near the mylonitic front. Geology, 18(3), 216-219.
Reynolds, S.J., Spencer, J.E., & DeWitt, E., (1987). Stratigraphy and U-Th-Pb geochronology of Triassic and Jurassic rocks in west-central Arizona, in Dickinson, W.R., and Klute, M.A., eds., Mesozoic rocks of central and southern Arizona and adjacent areas: Arizona Geological Society Digest, 18, 65-80.
Richard, S. M., Ballard, S. N., Boettcher, S. S., Hamilton, W. B., Hoisch, T. D., & Tosdal, R. M., (1994), Mesozoic Tectonics of the Maria Belt, west-central Arizona and southeastern California, in S. F. McGill and Ross, T. M., eds., Geological Investigations of an Active Margin. Edited by Geological Society of America Field trip Guidebook. San Bernardino, CA: County Museum Association, 1994, 272-292.
Royden, L. (1996). Coupling and decoupling of crust and mantle in convergent orogens: Implications for strain partitioning in the crust. Journal of Geophysical Research: Solid Earth, 101(B8), 17679-17705.
Royden, L., & Keen, C. E. (1980). Rifting process and thermal evolution of the continental margin of eastern Canada determined from subsidence curves. Earth and Planetary Science Letters, 51(2), 343-361.
Rosenberg, C.L. & Handy, M.R. (2005), Experimental deformation of partially melted granite revisited: implications for the continental crust. Journal of Metamorphic Geology, 23, 19-28. https://doi.org/10.1111/j.1525-1314.2005.00555.x
Ruppel, C., Royden, L., & Hodges, K. V. (1988). Thermal modeling of extensional tectonics: Application to pressure-temperature-time histories of metamorphic rocks. Tectonics, 7(5), 947-957.
Salem, A.C., (2009). Mesozoic tectonics of the Maria fold and thrust belt and McCoy basin an examination of polyphase deformation and synorogenic response, PhD Thesis: University of New Mexico, Dept. of Earth and Planetary Sciences, Albuquerque, NM, USA.
Scoggin, S. H., Chapman, J. B., Shields, J. E., Trzinski, A. E., & Ducea, M. N. (2021). Early Paleogene Magmatism in the Pinaleño Mountains, Arizona: evidence for crustal melting of diverse basement assemblages during the Laramide orogeny. Journal of Petrology, 62(12), egab095.
Searle, M. P. (2010). Low-angle normal faults in the compressional Himalayan orogen; Evidence from the Annapurna–Dhaulagiri Himalaya, Nepal. Geosphere, 6(4), 296-315.

Searle, M. P., & Lamont, T. N. (2020). Compressional metamorphic core complexes, low-angle normal faults and extensional fabrics in compressional tectonic settings. Geological Magazine, 157(1), 101-118.

Searle, M. P., & Lamont, T. N. (2022). Compressional origin of the Aegean orogeny, Greece. Geoscience Frontiers, 13(2), 101049.

Searle, M. P., & Rex, A. J. (1989). Thermal model for the Zanskar Himalaya. Journal of Metamorphic Geology, 7(1), 127-134.

Searle, M. P., Simpson, R. L., Law, R. D., Parrish, R. R., & Waters, D. J. (2003). The structural geometry, metamorphic and magmatic evolution of the Everest massif, High Himalaya of Nepal–South Tibet. Journal of the Geological Society, 160(3), 345-366.

Singleton, J. S., D. F. Stockli, P. B. Gans, & M. G. Prior (2014). Timing, rate, and magnitude of slip on the Buckskin-Rawhide detachment fault, west-central Arizona, Tectonics, 33, 1596–1615, doi:10.1002/2013TC003517.

Sláma, J., Košler, J., Condon, D. J., Crowley, J. L., Gerdes, A., Hanchar, J. M., ... & Whitehouse, M. J. (2008). Plešovice zircon—a new natural reference material for U–Pb and Hf isotopic microanalysis. Chemical geology, 249(1-2), 1-35.

Spear, F. S., & Pyle, J. M. (2002). Apatite, monazite, and xenotime in metamorphic rocks.

Spear, F. S., & Pyle, J. M. (2010). Theoretical modeling of monazite growth in a low-Ca metapelite. Chemical Geology, 273(1-2), 111-119.

Spencer, J. E., & Reynolds, S. J. (1990). Relationship between Mesozoic and Cenozoic tectonic features in west central Arizona and adjacent southeastern California. Journal of Geophysical Research: Solid Earth, 95(B1), 539-555.

Spencer, J. E., Richard, S. M., & Reynolds, S. J. (2024). Geologic map of the Little Harquahala Mountains, west-central Arizona (v. 2.0, DGM-203) [Map]. Arizona Geological Survey.

Strachan, R. A., (1994). Evidence in North-East Greenland for Late Silurian–Early Devonian regional extension during the Caledonian orogeny. Geology 22, 913–16

Strachan, R. A., & Martin M. W., (2001). Evidence for contemporaneous yet contrasting styles of granite magmatism during extensional collapse of the northeast Greenland Caledonides. Tectonics, 20, 458–73.

Strickland, E. D., Singleton, J. S., & Haxel, G. B. (2018). Orocopia Schist in the northern Plomosa Mountains, west-central Arizona: A Laramide subduction complex exhumed in a Miocene metamorphic core complex. Lithosphere, 10(6), 723-742.

Teyssier, C., & Whitney, D. L. (2002). Gneiss domes and orogeny. Geology, 30(12), 1139-1142.

Walsh, E. O., Wong, M. S., Singleton, J. S., Wrobel, A. J., Weiss, T., & Christensen, K. (2016). Evidence for polyphase exhumation of the Harcuvar metamorphic core complex, western Arizona. Geological Society of America Abstracts with Programs, 48(7), 287659. https://doi.org/10.1130/abs/2016AM-287659

Waters, D. J., Law, R. D., Searle, M. P., & Jessup, M. J. (2019). Structural and thermal evolution of the South Tibetan Detachment shear zone in the Mt Everest region, from the 1933 sample collection of LR Wager. Geological Society, London, Special Publications, 478(1), 335-372.

Watt, G. R., Kinny, P. D., & Friderichsen, J. D. (2000). U–Pb geochronology of Neoproterozoic and Caledonian tectonothermal events in the East Greenland Caledonides. Journal of the Geological Society, 157(5), 1031-1048.

Weinberg, R. F., & Hasalová, P. (2015). Water-fluxed melting of the continental crust: a review. Lithos, 212, 158-188.

Wells, M. L., & Hoisch, T. D. (2008). The role of mantle delamination in widespread Late Cretaceous extension and magmatism in the Cordilleran orogen, western United States. Geological Society of America Bulletin, 120(5-6), 515-530.

Whitney, D. L., Teyssier, C., Rey, P., & Buck, W. R. (2013). Continental and oceanic core complexes. Geological Society of America Bulletin, 125(3-4), 273-298.

Yang, L., Zeng, L., Wang, J., Gao, L., & Guo, C. (2019). Is Himalayan leucogranite a product by in situ partial melting of the Greater Himalayan Crystalline? A comparative study of leucosome and leucogranite from Nyalam, southern Tibet. Lithos, 344–345, 105124. DOI: 10.1016/j.lithos.2019.105124

White A. P., & Hodges K. V., (2002). Multistage extensional evolution of the central East Greenland Caledonides. Tectonics 21:1048

White A. P., & Hodges K. V., (2003). Pressure-temperature-time evolution of the central East Greenland Caledonides: quantitative constraints on crustal thickening and synorogenic extension. Journal of Metamorphic Geology, 21, 875–97

White AP, Hodges KV, Martin MW, & Andresen A. (2002). Geologic constraints on middle-crustal behavior during broadly synorogenic extension in the central East Greenland Caledonides. Interntional Journal of Earth Science, 91, 187–208.

Wiedenbeck, M. A. P. C., Alle, P., Corfu, F. Y., Griffin, W. L., Meier, M., Oberli, F. V., ... & Spiegel, W. (1995). Three natural zircon standards for U-Th-Pb, Lu-Hf, trace element and REE analyses. Geostandards newsletter, 19(1), 1-23.

Wong, M. S., Singleton, J. S., Seymour, N. M., Gans, P. B., & Wrobel, A. J. (2023). Late Cretaceous-Early Paleogene Extensional Ancestry of the Harcuvar and Buckskin-Rawhide Metamorphic Core Complexes, Western Arizona. Tectonics, 42(2), e2022TC007656.